STONELEY WAVE PROPAGATION ACROSS BOREHOLE PERMEABILITY HETEROGENEITIES

by

Xiaomin Zhao, M.N. Toksöz, and C.H. Cheng

Earth Resources Laboratory
Department of Earth, Atmospheric, and Planetary Sciences
Massachusetts Institute of Technology
Cambridge, MA 02139

ABSTRACT

An important application of borehole acoustic logging is the determination of formation permeability using Stoneley waves. Heterogeneous permeable structures, such as fractures, sand-shale sequences, etc., are commonly encountered in acoustic logging. The purpose of this study is to investigate the effects of the permeability heterogeneities on the borehole Stoneley wave propagation.

We have studied the effects of formation permeability heterogeneities on the Stoneley wave propagation when the heterogeneity changes in radial and azimuthal directions (Zhao et al., 1993). To further study the problem of acoustic logging in heterogeneous porous formations, we study the case where the formation permeability varies in the borehole axial and radial directions. This is a very important problem because vertical heterogeneity variations are commonly encountered in acoustic logging applications. Using the finite difference approach, such heterogeneities as random heterogeneous permeability variations, multiple fracture zones, permeable (sand) - non-permeable (shale) sequences, can be readily modeled, and the results are presented. Our numerical simulation results show that the continuous permeability variations in the formation have only minimal effects on the Stoneley wave propagation. Whereas the discontinuous variation (e.g., permeable sand and non-permeable shale sequences) can have significant effects on the Stoneley wave propagation. However, when the Stoneley wavelength is considerably large compared to the scale of heterogeneity variations, the Stoneley wave is sensitive only to the overall fluid transmissivity of the formation heterogeneity.

To demonstrate the effects of heterogeneity on the Stoneley wave propagation, an experimental data set (Winkler et al., 1989) has been modeled using a randomly layered permeability model. The heterogeneous permeability model results agree with the data very well, while the data disagree with the results from homogeneous permeability models.

The numerical technique for calculating Stoneley wave propagation across permeability heterogeneities has been applied to interpret the acoustic logging data across a heterogeneous fracture zone (Paillet, 1984). The modeling technique, in conjunction with a variable permeability model, successfully explains the non-symmetric patterns of the Stoneley wave attenuation and reflection at the top and bottom of the fracture

zone, while it is difficult to explain these patterns using a homogeneous permeable zone model. The technique developed in this study can be used as an effective means for characterizing permeability heterogeneities using borehole Stoneley waves.

INTRODUCTION

In a previous study, we investigated the effects of radial and azimuthal variations of formation permeability on the borehole Stoneley wave propagation (Zhao et al., 1993). In this paper, we will study the situation where the permeability varies in vertical (or borehole axial) and radial directions. This situation is commonly encountered in acoustic logging applications. For example, vertical layering of sedimentary rocks often results in formation sequences that consist of permeable and non-permeable layers (e.g., sand-shale sequences). Even in formations that are considered homogeneous, permeability values measured from well bores often show considerable variations. In many situations, formation permeability is due to fractures and/or permeable zones that intersect the borehole. The characterization of these permeability heterogeneities and the determination of their fluid transmissivity are very important tasks in acoustic logging applications (Paillet, 1984; Tang and Cheng, 1993), in which the borehole Stoneley wave is commonly used as a primary means for formation permeability studies.

The effects of vertical formation permeability heterogeneity variation on Stoneley wave propagation have been studied by numerous authors. Hornby et al. (1989), Tang and Cheng (1988), and Güler and Toksöz (1987) have studied the propagation of Stoneley waves across borehole fractures. Tang and Cheng (1993) presented a theory which can be used to study the effects of the permeable zone as well as those of fractures. Kostek (1991), by using a finite difference approach, studied the effects of multiple borehole fractures on Stoneley wave propagation. In this work, we will study a more general case in which the formation permeability can have arbitrary variations along the vertical as well as radial directions. As a result, permeability heterogeneities of interest, such as sand-shale sequences, heterogeneous permeable layers, multiple fractures etc., can be analyzed. The results of these numerical studies will not only demonstrate the effects of the permeability heterogeneities on the borehole Stoneley waves, but also can be used to provide theoretical bases for detecting and characterizing these heterogeneities using Stoneley wave measurements.

As discussed in Zhao et al. (1993), the effects of formation heterogeneity can be studied using a simplified Biot model approximation (Tang et al., 1991b). By decomposing the problem into the elastic and flow problems, we can solve the pore fluid flow problem for the heterogeneous porous formation independent of the elastic problem. The combination of the solution for the elastic and flow problems will give the solution for Stoneley wave propagation with heterogeneous permeability.

The behavior of dynamic fluid flow in heterogeneous porous media has been modeled (Zhao et al., 1992). Because of the dispersive nature of the flow motion, an iterative finite difference technique was developed to compute the flow field in the frequency domain. For the present borehole geometry, we need to solve the dynamic fluid flow

problem for the cylindrical coordinate system. The iterative finite difference technique for the cylindrical system has been developed (Zhao et al., 1993) to investigate dynamic fluid flow in formations with radial and azimuthal permeability variations. For the present study, formation permeability will vary along the borehole axial and radial directions. Therefore, the iterative finite difference technique used in Zhao et al., (1993) will be modified for the axial and radial coordinates system. Furthermore, because of heterogeneity variation along the axial direction and the resulting axial variation of Stoneley wave propagation, we will employ a propagator matrix method to compute the Stoneley wave propagation across the permeability heterogeneities.

The effects of the borehole permeability heterogeneity on the Stoneley wave propagation can be reflected from the transmission loss (or attenuation) and reflection from the heterogeneity boundaries. Both laboratory and field studies have provided such evidence. In the laboratory, the effects of heterogeneity on Stoneley wave propagation have been noticed by Winkler et al., (1989). They evaluated the theory of Stoneley wave propagation in porous boreholes using laboratory experiments and found excellent agreement between theory and experiment for 3 out of 4 data sets. However, they reported that for one data set the data disagree with the results predicted using the homogeneous model theory. They suggested that sample heterogeneity was the cause of this discrepancy.

In the field study, effects of permeability heterogeneity are commonly encountered in acoustic logging across fractures or fracture zones. Even in isolated fracture zones, the permeability may have significant variations and these variations can have important effects on the Stoneley wave propagation. Such a case was observed by Paillet (1984), who reported an acoustic logging data set across a permeable fracture zone. The data set shows non-symmetric patterns for Stoneley wave attenuation and reflection at the upper and lower boundaries of the fracture zone. Although Tang et al. (1991a) have used a homogeneous permeability layer to model the fracture zone and explained the significant Stoneley wave attenuation and reflection, the homogeneous layer cannot model the heterogeneity variation within the zone and cannot explain the non-symmetric patterns.

With the numerical analysis developed in this study, we will carry out modeling studies on the laboratory data set of Winkler et al. (1989) and the field data set of Paillet (1984). These studies will demonstrate the effects of formation heterogeneity on Stoneley wave propagation and the applicability of the numerical technique in handling formation heterogeneities.

STONELEY WAVE PROPAGATION IN A FORMATION WITH VARIABLE PERMEABILITIES

As shown in Zhao et al. (1993), for a Stoneley wave propagating in a permeable porous borehole, the interaction of the Stoneley wave with the formation can be decomposed into two parts (Tang et al., 1991b). The first is the interaction with an equivalent elastic formation, and the second is the interaction with the dynamic fluid flow into the formation. The Stoneley wave can be described by the following one-dimensional wave

equation (Zhao et al., 1993):

$$\frac{d^2P}{dz^2} + \left[\frac{\omega^2}{v_f^2} + \frac{2\rho_f\omega^2}{R_0}\frac{U_e}{P} + \frac{2\rho_f\omega^2}{R_0}\frac{U_f}{P}\right]P = 0 \ , \tag{1}$$

with the Stonely wavenumber k given by

$$k = \sqrt{\frac{\omega^2}{v_f^2} + \frac{2\rho_f\omega^2}{R_0}\frac{U_e}{P} + \frac{2\rho_f\omega^2}{R_0}\frac{U_f}{P}} \ . \tag{2}$$

This equation indicates that the Stoneley wave propagation in a porous borehole is affected by the formation elastic displacement U_e and the pore fluid flow displacement U_f. If the borehole wall is impermeable, i.e., $U_f = 0$, then the Stoneley wavenumber can be written as

$$k_e = \sqrt{\frac{\omega^2}{v_f^2} + \frac{2\rho_f\omega^2}{R_0}\frac{U_e}{P}} \ . \tag{3}$$

Because the objective of the present study is to study the effects of permeability variation, we neglect the variation of the elastic properties and assume a spatially invariable k_e for the formation. For the given k_e, the Stoneley wavenumber in a permeable borehole is

$$k = \sqrt{k_e^2 + \frac{2\rho_f\omega^2}{R_0}\frac{U_f}{P}} \ . \tag{4}$$

Equation (4) is valid only for a formation with homogeneous permeability. For a formation with heterogeneous permeability that can change with the axial distance z, U_f will also vary with z. In this case, we discretize the borehole (along the axial direction) into equally-spaced intervals. Within each small interval, permeability can be regarded as homogeneous and Equation (4) can be used to calculate the Stoneley wavenumber for each interval. To find this vertically variable $k(z)$, we will use the finite difference method to solve for $U_f(z)$. The overall effects of the permeability variation will be calculated using a propagator matrix technique.

Dynamic Fluid Flow in the Radial and Axial Coordinate System

The dynamic fluid flow in heterogeneous permeability media is described by the following equation (see Zhao *at al.*, 1992)

$$\nabla \cdot [\alpha(\omega, \vec{x})\nabla p] + i\omega p = 0 \ , \tag{5}$$

where p is dynamic pressure associated with pore fluid motion,

$$\alpha(\omega, \vec{x}) = \frac{\kappa(\omega, \vec{x})K_f}{\phi\mu(1+\xi)} \tag{6}$$

is dynamic pore fluid diffusivity, K_f = fluid incompressibility, ϕ = porosity, μ = fluid viscosity, and ξ is a correction for solid matrix compressibility (Norris, 1989). The

fluid diffusivity $\alpha(\omega, \vec{x})$ is a function of both frequency and the spatial position $\vec{x}$. This happens if the dynamic permeability (Johnson et al., 1987)

$$\kappa(\omega, \vec{x}) = \frac{\kappa_0(\vec{x})}{\left(1 - \frac{i}{2}\tau\kappa_0(\vec{x})\rho_0\omega/\mu\phi\right)^{\frac{1}{2}} - i\frac{\tau\kappa_0(\vec{x})\rho_0\omega}{\mu\phi}} \tag{7}$$

is a function of the spatial position when the static permeability $\kappa_0(\vec{x})$ varies with $\vec{x}$. In Equation (7), τ is tortuosity of the porous medium, ρ_0 the pore fluid density.

For the borehole configuration, the cylindrical coordinates are most convenient to use. In this study, we investigate a two and half- dimensional (2.5D) case where the permeability variation is in the radial (r) and vertical (z) directions, i.e.,

$$\kappa_0(\vec{x}) = \kappa_0(r, z) \ , \tag{8}$$

but the pore fluid flow takes place in the 3-D space. In the cylindrical system, Equation (5) becomes

$$\frac{\partial}{\partial r}\left(\alpha(r,z)\frac{\partial p}{\partial r}\right) + \frac{\alpha(r,z)}{r}\frac{\partial p}{\partial r} + \frac{\partial}{\partial z}\left(\alpha(r,z)\frac{\partial p}{\partial z}\right) + i\omega p = 0 \tag{9}$$
$$(r > R_0 \text{ and } 0 < z < L)$$

where R_0 is the borehole radius and $z = 0$ and $z = L$ represent the lower and upper boundaries of the heterogeneous formation, respectively. The boundary conditions for Equation (9) are described below.

The boundary condition at the borehole wall is the continuity of pressure, i.e., the borehole Stoneley wave pressure should equal the pore fluid pressure at the borehole wall. However, the Stoneley wave pressure is not known at this stage. We therefore use a perturbation approach. We assume that the Stoneley pressure can be decomposed into two parts. The first is the zero order term $p_0 e^{ik_e z}$, which corresponds to the equivalent elastic (or non-permeable) formation, with p_0 being the pressure amplitude. The second part is a perturbation term due to the porous formation fluid flow. The borehole Stoneley wave pressure is then written as

$$p = p_0 e^{ik_e z} + p_1 \ . \tag{10}$$

Compared with the pore fluid flow due to $p_0 e^{ik_e z}$, the pore fluid flow associated with p_1 is a higher order perturbation because p_1 itself is the first order perturbation. Therefore, for a first order perturbation theory (i.e., the simplified Biot model of Tang et al., 1991b), we assign the known zero order Stoneley wave pressure function $p_0 e^{ik_e z}$ as the boundary condition for the pore fluid flow pressure at the borehole wall,

$$p(R_0, z) = p_0 e^{ik_e z} \ , \qquad (0 < z < L) \tag{11}$$

together with the radiation condition

$$p(r = \infty, z) = 0 \tag{12}$$

and the no-flow boundary conditions

$$\frac{\partial p(r, z=0)}{\partial z} = \frac{\partial p(r, z=L)}{\partial z} = 0 \ . \tag{13}$$

With these boundary conditions, Equation (9) is solved using the iterative finite difference technique (see Appendix) to give the pore pressure distribution over the (r, z) grid. The fluid flow at the borehole wall is computed using the modified Darcy's law (Tang et al., 1991b)

$$-i\omega U_f(z) = -\frac{\kappa(\omega; r, z)}{\mu} \frac{dp(r, z)}{dr}\bigg|_{r=R_0} \ . \tag{14}$$

Note this flow is a function of z because of the permeability variation. The pressure gradient is numerically evaluated from the calculated pressure field at the borehole wall. With this flow field, the Stoneley wave propagation will be perturbed. We then add this perturbation to the elastic Stoneley wavenumber k_e to give the Stoneley wavenumber in the heterogeneous formation using Equation (4)

$$k(z) = \sqrt{k_e^2 + \frac{2\rho_f \omega^2}{R_0} \frac{U_f(r, z)}{p(r, z)}\bigg|_{r=R_0}} \ . \tag{15}$$

Because the flow field at the borehole boundary ($r = R_0$) varies with z, the resulting permeable formation Stoneley wavenumber is also a function of z. The effects of this variable wavenumber on the Stoneley wave propagation will be addressed in the following.

Propagation using the propagator matrix method

To calculate the effects of the heterogeneous fluid flow field on the Stoneley wave propagation, we use the propagator matrix technique (Aki and Richards, 1980). For the wavenumber $k(z)$ given in Equation (15), the borehole Stoneley wave pressure $p(z)$ and vertical displacement $u(z)$ are

$$p(z) = \rho_f \omega^2 A(z) e^{ik(z)z} \tag{16}$$

$$u(z) = ik(z) A(z) e^{ik(z)z} \tag{17}$$

where $A(z)$ is the as-yet-to be determined amplitude coefficient, $A(z)e^{ik(z)z}$, representing the Stoneley wave displacement potential. To our advantage, the finite difference grid along the z-direction discretizes the borehole into equally-spaced layers of thickness δz. The continuity conditions for pressure and displacement are then applied to each interface between the adjacent layers. At each boundary, a 2×2 boundary condition matrix D is calculated which can be used to propagate the displacement-pressure vector $[u, p]^T$ along the borehole axis. For example, at $z = z_n$, D is given as

$$D_n(z_n) = \begin{pmatrix} e^{ik(z_n)z_n} & e^{-ik(z_n)z_n} \\ \\ \dfrac{i\rho_f\omega^2}{k(z_n)} e^{ik(z_n)z_n} & \dfrac{-i\rho_f\omega^2}{k(z_n)} e^{-ik(z_n)z_n} \end{pmatrix} \ . \tag{18}$$

The propagation of the vector $[u,p]^T$ across the discretized borehole layers is expressed as

$$\begin{pmatrix} u \\ p \end{pmatrix}_{z=0} = \left(\prod_{n=1}^{N} D_n(z_n) D_n^{-1}(z_{n-1}) \right) \begin{pmatrix} u \\ p \end{pmatrix}_{z=L} = G \begin{pmatrix} u \\ p \end{pmatrix}_{z=L} , \tag{19}$$

where N is the number of the finite difference gridpoints along z-direction, L is the total propagation length, and G is the notational simplification of the matrix product in Equation (19). Using the expression of D, the propagation matrix of layer n is written as

$$D_n(z_n) D_n^{-1}(z_{n-1}) = \begin{pmatrix} cos[k(z_n)\delta z] & sin[k(z_n)\delta z] \frac{k_n}{\rho_f \omega^2} \\ -sin[k(z_n)\delta z] \frac{\rho_f \omega^2}{k_n} & cos[k(z_n)\delta z] \end{pmatrix} \tag{20}$$

where $k_n = k(z_n)$ is the Stoneley wavenumber at $z = z_n$ computed using Equation (15).

Using the propagator matrix technique, the transmission and reflection of a Stoneley wave due to a heterogeneous permeable structure can be calculated. Let a Stoneley wave $A_0^+ e^{ik_e z}$ approach from $z < 0$ onto the upper boundary of the heterogeneous zone (z = 0). Upon interacting with the structure, part of the wave energy will be reflected back, propagating in the negative z direction as given by $A_0^- e^{-ik_e z}$. Across the lower boundary at $z = L$, there is only the transmitted wave, given by $A_N^+ e^{ik_N z}$, where k_N is the Stoneley wavenumber for the formation located adjacent to the $z = L$ boundary. k_N can be taken as k_e, assuming that the formations above and below the heterogeneous formation are the same. Therefore, the displacement and pressure at $z = 0$ and $z = L$ are

$$\begin{cases} u = ik_e(A_0^+ - A_0^-) \\ p = \rho_f \omega^2 (A_0^+ + A_0^-) \end{cases} \qquad (\mathrm{z} = 0) \tag{21}$$

and

$$\begin{cases} u = ik_N A_N^+ e^{ik_N L} \\ p = \rho_f \omega^2 A_N^+ e^{ik_N L} \end{cases} \qquad (\mathrm{z} = \mathrm{L}) \tag{22}$$

respectively.

Equations (21) and (22) are related using the propagator matrix method [Equation (19)],

$$\begin{pmatrix} ik_e(A_0^+ - A_0^-) \\ \rho_f \omega^2 (A_0^+ + A_0^-) \end{pmatrix} = \begin{pmatrix} g_{11} & g_{12} \\ g_{21} & g_{22} \end{pmatrix} \begin{pmatrix} ik_N A_N^+ e^{ik_N L} \\ \rho_f \omega^2 A_N^+ e^{ik_N L} \end{pmatrix} \tag{23}$$

where g_{ij} (i,j = 1, 2) is the element of G. Solving this equation, we find the transmission and reflection coefficients for the pressure field,

$$\begin{aligned} Trs &= \frac{p^+|_{z=L}}{p^+|_{z=0}} \\ &= \frac{(ik_e g_{11} + \rho_f \omega^2 g_{12})(\rho_f \omega^2 g_{22} - ik_e g_{21}) - (ik_e g_{21} + \rho_f \omega^2 g_{22})(\rho_f \omega^2 g_{12} - ik_e g_{11})}{ik_N(\rho_f \omega^2 g_{22} - ik_e g_{21}) - \rho_f \omega^2 (\rho_f \omega^2 g_{12} - ik_e g_{11})} \end{aligned} \tag{24}$$

$$Ref = \frac{p^-|_{z=0}}{p^+|_{z=0}}$$

$$= \frac{\rho_f\omega^2(ik_eg_{11}+\rho_f\omega^2g_{12})-ik_e(ik_eg_{21}+\rho_f\omega^2g_{22})}{ik_N(\rho_f\omega^2g_{22}-ik_eg_{21})-\rho_f\omega^2(\rho_f\omega^2g_{12}-ik_eg_{11})} \quad . \tag{25}$$

Therefore, by using the finite difference method to compute the fluid flow effects for the heterogeneous formation, and the propagation matrix method to calculate the propagation for the spatially variable Stoneley wavenumber $k(z)$, Stoneley wave propagation across an arbitrarily heterogeneous permeable structure can be modeled. This allows us to model the effects of such heterogeneity structures as multiple permeable zones, sand-shale (permeable and non-permeable) sequences, or any permeable structure with varying permeability values.

In formations where the scale of permeability variation is small compared to the wavelength, the propagator matrix method can be used to obtain an equivalent Stoneley wavenumber for the heterogeneous formation. In the heterogeneous formation, the transmitted Stoneley wave at $z = L$ is $A(L)e^{ik(L)L}$ where $k(L)$ is computed using the finite difference method and $A(L)$ is computed using the propagator matrix method. Assume that this wave can be approximated by a wave $A_0e^{i\bar{k}L}$, where A_0 is the wave amplitude at $z = 0$ and $\bar{k}$ is the equivalent Stoneley wavenumber. Equating $A_0e^{i\bar{k}L}$ with $A(L)e^{ik(L)L}$, we have

$$\bar{k} = k(L) - \frac{i}{L}ln\left(\frac{A(L)}{A_0}\right). \tag{26}$$

From this equivalent wavenumber, the Stoneley wave attenuation $1/Q$ and phase velocity v_{st} are computed using

$$\begin{cases} 1/Q &= 2\dfrac{Im(\bar{k})}{Re(\bar{k})} \\ v_{st} &= \dfrac{\omega}{Re(\bar{k})} \end{cases} \quad . \tag{27}$$

NUMERICAL SIMULATION RESULTS

In this section, we present the finite difference simulation results for various permeability heterogeneities along a vertical borehole. For all the calculations below, we first calculate the elastic problem using the saturated rock properties: $v_p = 4000$ m/s, $v_s = 2300$ m/s, and $\rho = 2.65$ g/cm^3. The Stoneley wavenumber k_e for the equivalent elastic formation is calculated using the borehole dispersion equation (Cheng and Toksöz, 1981). The borehole fluid density and velocity are $\rho_f = 1$ g/cm^3 and $v_f = 1500$ m/s, respectively. The borehole radius is 0.1 m. For simplicity, we assume that the elastic properties for the various heterogeneous permeability distributions are the same, so that the same k_e is used for the following cases. In all the cases below (unless specified), the pore fluid properties are: $K_f = 2.25$ GPa, $\rho_0 = 1$ g/cm^3, $\mu = 1.14$ cp, porosity $\phi = 0.2$, and tortuosity $\tau = 3$.

Homogeneous Permeability – A Test of the Numerical Algorithm

We first present the simulation result for a homogeneous permeable formation surrounding the borehole. This example, together with the existing analytical solution, offers a test of the validity and accuracy of the finite difference simulation algorithm.

Figure 1 shows the comparison between the Stoneley wave phase velocity (a) and attenuation (b) calculated using the analytical solution (see Zhao et al., 1993) and those using the finite difference method, and equivalent wavenumber formula (Equation 26) for a homogeneous permeability model. These results are calculated for the frequency range of $0 \sim 5$ kHz in which most Stoneley wave measurements are performed. The formation permeability is 1 Darcy. For simplicity, the effects due to solid matrix compressibility are neglected (i.e., $\xi = 0$ in Equation 6) when calculating both the analytical and finite difference results. The results for the two different approaches are in excellent agreement. This comparison demonstrates the validity and accuracy of the finite difference technique. Therefore, in the case of a heterogeneous permeability distribution where an analytical solution is difficult to find, we will rely on the finite difference method to calculate the Stoneley wave propagation.

Variable Permeability Models

In the field acoustic logging applications, the formation permeability is usually heterogeneous. For example, the permeability may fluctuate from place to place due to random variations. The permeability may have cyclic variations due to sand-shale sequences. The effects of these heterogeneity variations on the borehole Stoneley wave propagation are studied here. In this section, we assume that the logging tool is within the heterogeneous formation and we will analyze the average Stoneley wave attenuation and velocity dispersion characteristics using Equations (26) and (27).

In Figures 2, 3, and 4, three formation permeability heterogeneity models are shown. They are the 2-D random variation with a Gaussian correlation function of correlation length of 0.2 m (Figure 2), the 1-D random variation along borehole axial direction with Gaussian correlation function of correlation length 0.1 m (Figure 3), and the permeable and non-permeable layer model generated using the Poisson process. All three models have the same average permeability of 1 Darcy. For the continuous models, the standard deviation of the variation is 30%. For the discontinuous model, the permeability contrast between high and low permeability layers is 100:1. For the borehole Stoneley wave, the axial propagation distance is much greater than the depth of fluid motion penetration in the radial direction. We therefore set the axial and radial model dimensions as 10 m and 1 m, respectively. In Figures 2, 3, and 4, the models are shown only for a 5 m section in the axial direction. In these figures, the calculated dynamic fluid pressure amplitude distribution for those heterogeneous models is also plotted. The frequency for the fluid motion is 1 kHz. As can be seen from these figures, the formation fluid pressure distributions are distinctly different from one another because of the different heterogeneity variations. The 2-D random model shows considerable fluid pressure variation in both radial and axial directions. The 1-D model shows less axial

variations. For the discontinuous model, the fluid motion is largely concentrated in the high permeability layers.

The effects of the heterogeneity variations are now analyzed. We use Equations (26) and (27) to calculate the average Stoneley wave phase velocity and attenuation for these heterogeneity models and plot the results in Figure 5 (a) (velocity) and (b) (attenuation) in the frequency range of 0 - 5 kHz. For comparison, the results for a homogeneous formation with a constant permeability of 1 Darcy is also shown. A very interesting feature of these results is that, despite the considerable difference in the heterogeneous variations, the average Stoneley wave attenuation and velocity dispersion are very close to the homogeneous model results. Only the discontinuous model results show appreciably lower attenuation and velocity dispersion compared to the homogeneous model results.

The difference between the discontinuous model and the continuous model results becomes very significant when formation permeability is high. To demonstrate this, we have re-calculated the Stoneley wave attenuation and phase velocity for the same heterogeneous models shown in Figures 2, 3, and 4 by increasing the average model permeability from 1 Darcy to 10 Darcy and keeping other parameters (porosity, tortuosity, etc.) unchanged. The results are shown in Figure 6 for the Stoneley wave velocity (Figure 6 a) and attenuation (Figure 6 b). The continuous heterogeneous model results, despite some small differences, are still close to the homogeneous model results. However, the discontinuous model results show significant differences from the continuous and homogeneous model results. The velocity is higher than those from the other models in the frequency range of 0 - 2 kHz and the attenuation is significantly lower than those from the other models.

The difference between discontinuous and continuous permeability models at high permeabilities can be explained based on the behavior of dynamic permeability. In both models, the Stoneley wave propagation sums all the fluid flow effects over the same model length. In the discontinuous model, only the high permeability layers contribute to the Stoneley wave attenuation and dispersion. However, at high permeability values, the dynamic permeability is less sensitive to permeability as can be seen by its asymptotic behavior $\kappa(\omega) \overset{\kappa_0 \to \infty}{\longrightarrow} \frac{i\mu\phi}{\tau\rho_0\omega}$; there is no sensitivity to permeability κ_0 when κ_0 is very high. Therefore, compared to the continuous model, the high permeability layers in the discontinuous model will contribute less to the attenuation and dispersion when averaged over the same propagation length. For the continuous model, because there is no significant permeability contrast, the average result will be more or less close to the homogeneous result.

STONELEY WAVE PROPAGATION ACROSS HETEROGENEOUS PERMEABLE STRUCTURES

In this section, we study Stoneley wave propagation across various heterogeneous permeable structures. This is an important problem for the characterization of formation permeability using borehole Stoneley wave measurements. A theory has been presented

by Tang and Cheng (1993) to model borehole fractures as a highly permeable zone. This theory is able to explain the observed Stoneley wave transmission and reflection at fractures. A drawback of this model is that it uses a homogeneous permeability layer to model the permeable zone and therefore neglects the permeability variation within the zone. In reality, a natural permeable structure may contain various heterogeneous structures. With the heterogeneous propagation theory developed in this study, we can study the effects of the heterogeneity structures and compare the similarity and difference between the simple homogeneous model and the heterogeneity structure model.

Comparison with the Homogeneous Permeable Zone Model

According to Tang and Cheng (1993), the Stoneley wave transmission and reflection coefficients due to a homogeneous permeable layer are given by

$$Trs = \frac{4k_1k_2e^{-ik_2L}}{(k_1+k_1)^2e^{-ik_2L}-(k_1-k_2)^2e^{ik_2L}} \tag{28}$$

$$Ref = \frac{2i(k_2^2-k_1^2)sin(k_2L)}{(k_1+k_2)^2e^{-ik_2L}-(k_1-k_2)^2e^{ik_2L}} \tag{29}$$

where k_1 is the Stoneley wavenumber outside the permeable zone, k_2 is the permeable zone Stoneley wavenumber, and L is the zone thickness. In fact, the simple homogeneous permeable model results can be derived as the special case for the propagator matrix results (Equations 24 and 25). Therefore, the analytical results presented in Equations (28) and (29) can be used to test the validity and accuracy of the finite difference and propagator matrix approach developed in this study.

Figure 7 compares the transmission and reflection coefficients computed using the analytical results (Equations 28 and 29) and the numerical simulation results (Equations 24 and 25). The permeable zone has a porosity of 0.3, tortuosity of 3, permeability of 5 Darcy, and a thickness of 0.5 m. As can be seen from Figure 7, the results from the analytical approach and the numerical approach agree very well. Only at frequencies beyond 5 kHz, do the two transmission coefficients differ slightly. This comparison shows the validity and accuracy of our numerical modeling. In the case of a heterogeneous permeability structure, we can use our numerical technique to compute the Stoneley wave transmission and reflection due to the structure.

Double Permeable Layers

A permeable zone encountered in acoustic logging may consist of multiple permeable structures. The permeable zone with multiple structures results in some complex features compared to the single permeable layer model. For simplicity, we model the effects for a double permeable layer model (Figure 8). In this model two permeable layers, each having a permeability of 10 Darcy, porosity of 0.3, and thickness of 0.15 m are separated by a non-permeable formation of thickness 0.2 m. The high permeability value (10 Darcy) used here is based on the conclusion of Tang and Cheng (1993) that fracture zones can be modeled as high permeability layers.

The numerical finite difference technique, together with the propagation matrix method, is applied to model the Stoneley wave propagation across the double layer structure. The transmission and reflection coefficients calculated using the numerical method are plotted in Figure 9 for the frequency range from 0 to 5 kHz. For comparison, the results calculated for a single layer of thickness 0.3 m with the same permeability and porosity as the double layer model are also plotted (dashed curves). Although the double layer model and the single layer model have the same fluid transmissivity (permeability $\times$ thickness), the double layer results show more complex features compared with the single layer results. The transmission coefficient for the double layer model is somewhat lower than the single layer result due to the interaction of the two permeable layers. This interaction is especially pronounced for the reflection coefficient, resulting in the significant variation of the reflected wave amplitude in the frequency range being modeled. Moreover, in the frequency range of 2 to 3 kHz, the reflection coefficient can reach the value of 0.3, which is significantly higher than the value of the single layer result. The high amplitude reflected Stoneley wave events on an acoustic waveform log may be helpful in detecting two major fractures that are close to each other. It is also interesting to note that the transmission and reflection coefficients for the two layer and single layer models converge at very low frequencies, indicating that at very long wavelengths the Stoneley wave cannot resolve the structure of a heterogeneous zone, but is sensitive only to the overall fluid transmissivity of the zone.

Multiple Layer Structure

We study the effects of a permeable zone that consists of a sequence of permeable and non-permeable layers. The thicknesses of these layers are small compared to the Stoneley wavelength of interest. Figure 10 shows an example of such a model. The model is generated using a random repetition of layers of low and high permeabilities (they are 20 and 0.1 Darcy, respectively). The average thickness of the layers is 0.025 m, and thickness of the layers obeys the Poisson distribution (see Zhao and Toksöz, 1991).

The calculated Stoneley wave transmission and reflection coefficients are shown in Figure 11, together with the results for a single layer of the same thickness 0.4 m and a cumulative permeability of 10 Darcy. Compared to the homogeneous layer results, the Stoneley wave transmission coefficient is significantly higher than 2 kHz, and the reflection coefficient shows some complex features. The smaller transmission loss of the multiple layer model is consistent with the smaller average attenuation of the model shown in Figure 6, which is due to the same cause we discussed in relation to this figure. The reflection coefficient is very different from the homogeneous model result at higher frequences ($>$ 2 kHz). It decreases, then increases with frequency, showing that at high frequencies the reflection from the multiple layered zone is very sensitive to the fine structure of the zone. At low frequencies ($<$ 1 kHz) the homogeneous and heterogeneous model results approach each other. Compared to the double layer model results at low frequencies, we see again that very low frequency Stoneley waves see only the overall fluid transmissivity of a permeable zone, regardless of the fine structure of the zone.

Random Permeability Structure

We now study the case where the permeability within the permeable zone can have random but continuous variations. We model this situation using the 1-D continuous random model generated using the 1-D Gaussian correlation function (see Zhao and Toksöz, 1991). The permeability variation is shown in Figure 12 which has an average value of 10 Darcy and a standard deviation of 28%. This permeability variation is assigned to a permeable zone 0.4 m thick with a porosity value of 0.3. Figure 13 shows the resulting Stoneley wave transmission and reflection coefficients across the heterogeneous zone. For comparison, we also plot the results (dashed curves) calculated using a homogeneous layer model (Equations 28 and 29), in which we used the average permeability of 10 Darcy and the same thickness of 0.4 m for the layer.

Despite the considerable permeability variation within the permeable zone, the heterogeneous model results are not very different from the homogeneous model results, except the transmission and reflection coefficients for the heterogeneous model are a little higher than the homogeneous model result beyond 2 kHz. At low frequencies, especially approaching the zero frequency, the results from both models converge toward each other. This convergence occurs at higher frequency than the previous double layer and multiple layer models.

Model Comparison

To further investigate the similarity and difference of Stoneley wave propagation across the different heterogeneity models, we plot the Stoneley wave amplitude change versus distance across the permeable zone in Figure 14 for these models. The amplitude *vs.* distance curves are calculated for a 5 kHz Stoneley wave using the propagator matrix method to compute the transmitted wave amplitude Equation (24) at each finite difference grid inside the permeable zone.

We compare three situations: (1) the multiple layer structure given in Figure 10; (2) the random permeability variation model given in Figure 12; and (3) the homogeneous layer model. The parameters for all three models are the same (i.e., same porosity, thickness, and average permeability, etc). As shown in Figure 14, when the Stoneley wave enters the permeable zone, the amplitude begins to decrease. For the random permeability model, although the heterogeneous variation is evident on the amplitude, the overall result (dashed line) is not very different from the homogeneous model result, because of the continuous permeability variation. For the multiple layer model, which has a discontinuous permeability variation, the amplitude *vs.* distance curve is distinctly different from the homogeneous and the continuous model results. The amplitude is attenuated in the permeable layer, but remains constant in the non-permeable layers, resulting in a step-like decrease of the wave amplitude. As a result, the total amplitude reduction is less than those of the other two models. This result is also consistent with the Stoneley wave attenuation results plotted in Figure 6 which show that for the same average permeability the discontinuous permeability model has lower attenuation than those from the continuous models.

In the following application section, we will use the discontinuous permeability model to study the laboratory and field Stoneley wave data, which could not be explained using the homogeneous model theory. We will show that only the discontinuous permeability model theory can explain the data very well.

APPLICATION TO ACOUSTIC LOGGING DATA FROM HETEROGENEOUS FORMATIONS

Data from Laboratory Experiments

Winkler et al. (1989) were the first to perform laboratory experiments to evaluate Biot's theory for acoustic propagation in a porous borehole. Four samples were measured in their experiments. Three were synthetic materials made of resin-cemented glass beads (sample A, B, and C). One was a rock sample made of Berea sandstone (sample S.S.). All these samples were cylindrical in shape with a diameter of 21.6 cm. A borehole was drilled along the sample axis. The diameter of the hole was 1.06 cm for the synthetic samples and 0.95 cm for the rock sample. They showed the experimental results on Stoneley wave propagation in those permeable porous materials. For 3 samples (samples A, C, and S.S.), they found excellent agreement between theory and experiment. However, for one sample (sample B), the measured Stoneley wave velocity and attenuation were found to significantly deviate from the theoretical prediction. In a recently published paper, Tang *et al.* (1991a) applied the simplified Stoneley propagation model to Winkler et al.'s experimental data. Again, they found excellent agreement between theory and experiment for the 3 samples (A, C, and S.S.) and disagreement for sample B. The sample and fluid properties are summarized in Table I for reference. The comparison between the modeling results of Tang et al. (1991a) and experimental data is shown in Figure 15, in which both the Stoneley wave attenuation and phase velocity are over-estimated by the theory. Winkler et al. (1989) suggested that the discrepancy between the theory and experiment was due to the heterogeneities in the sample. With the theory of Stoneley wave propagation in heterogeneous formations developed here, we can test this hypothesis by modeling the laboratory data using heterogeneous permeability models.

We use the measured parameters given in Table I. From the measured rock and fluid density, velocity, and incompressibility, we use the formula of Norris (1989) to calculate the solid rock frame compressibility correction term ξ, which gives $\xi = 0.264$. We use this ξ value in Equation (6) for numerical modeling. From the formation and fluid acoustic properties and borehole diameter, we calculate the equivalent elastic formation Stoneley wavenumber k_e.

We now discuss the choice of heterogeneous permeability models. The constraint on these models is that the average permeability must equal the permeability value (2.3 Darcy) measured from the sample. A natural model choice is the random media model which has a mean value of 2.3 Darcy and the permeability fluctuates around this value with specified deviation (i.e., the continuous model described in Zhao and Toksöz, 1991). However, the modeling results in Figures 5 and 6 indicate that the continuous

permeability model results do not differ greatly from the homogeneous model results. Based on the modeling results, we exclude these models from the candidacy. On the other hand, the discontinuous permeability model results in these figures (especially Figure 6) show significantly less attenuation and dispersion compared with the homogeneous model results, as is also the case for the data shown in Figure 15. We therefore choose the 1-D discontinuous model to model the experimental data.

In our modeling, the numerical model length L is taken as 0.2 m, which is approximately the array aperture spanned by the scanning receiver in the experiment (Winkler et al., 1989). The radial model size is about 10 times that of the borehole diameter. The heterogeneous permeability model is generated using the Poisson process with an average thickness of 0.01 m. The high permeability layers have a permeability value of 4.6 Darcy, while the low permeability layers, 0.01 Darcy; the average is about 2.3 Darcy.

The modeled Stoneley wave velocity and attenuation are shown together with the measured data in Figure 16. There is excellent agreement between theory and data. It is worthwhile to note that this agreement holds for both phase velocity and attenuation. It is also worthwhile to point out that the same excellent agreement was obtained when different 1-D Poisson models with different average layer thicknesses are used in the numerical modeling. In these models, 50% of the formation has high permeability and the other 50%, low permeability.

Our numerical modeling results support the hypothesis of Winkler *et al.* (1989) that the sample heterogeneity was the cause of discrepancy between experimental data and theory for a homogeneous formation. In addition, our modeling also suggests that the effects of the heterogeneities are such that some portions of the borehole are very permeable and other portions are impermeable, similar to the Poisson layering models used in the numerical modeling.

Data from the URL-M11 Well

In this section, we apply the theory of Stoneley wave propagation across permeability heterogeneities to the acoustic logging data obtained from the URL-M11 well. This example demonstrates that the numerical modeling of the logging data not only will help determine the fluid transmissivity of a permeable fracture zone, but also assesses the distribution of permeability across the fracture zone.

The data set was obtained in a borehole (M11 well) at the Underground Research Laboratory (URL) located on the southern edge of the Canadian shield in Southeastern Manitoba, Canada. A major isolated fracture zone was detected at a depth of about 188 m in this borehole. Figure 17 shows the televiewer log, the Stoneley waveform data, and the Stoneley amplitude log data (open circles) in the vicinity of the fracture. In this figure, the modeling synthetic Stoneley wave waveform and amplitude log (solid line) of Tang et al. (1991a) using the simple homogeneous permeability layer model Equations 28 and 29) are also shown. The isolated fracture appeared in a single subhorizontal band on the televiewer log, but additional high resolution televiewer logs indicated that this fracture was actually composed of several subparallel fractures. The

logging waveforms were obtained using a sparker source at 5 kHz; the borehole and the tool diameters were 15.2 and 5.1 cm, respectively. The source-receiver spacing was 2.14 m.

As seen from the logging waveforms, the Stoneley waves are significantly attenuated across the fractures. A Stoneley wave reflection at the top can also be observed, as indicated by the line drawn on the waveform logs in Figure 17, which marks the moveout of the reflected waves. A feature that is of special interest in this study is that the field data do not have a clearly traceable down-going reflection, whereas the homogeneous layer theory of Tang et al. (1991a) predicts a symmetric pattern for the up-going and down-going reflections (Figure 17, synthetic waveform logs). The non-symmetric nature inherent in the logging data can also be seen from the Stoneley wave transmission log across the fracture zone.

The Stoneley wave transmission log is measured as the amplitude deficit or attenuation across the fracture. This measurement has long been used in fracture detection and characterization (Paillet, 1980). To compute the attenuation, one first applies a window that contains Stoneley arrivals. Then the mean square wave energy (sum of the square of each sampled wave amplitude within the window) is computed and modified by a half cosine taper. The attenuation or transmission log is measured from the amplitude deficit - the "representative" percentage decrease of the average wave energy in the time window over the vertical distance of one source-receiver separation. The transmission log obtained in this way gives a measure of the square of the transmission coefficient around the measurement frequency (Tang et al., 1991a).

The amplitude deficit log in Figure 17 was modeled by Tang et al. (1991a) using the homogeneous layer model (Equations 28 and 29). The model parameters were: permeability = 2.5 Darcy, porosity = 0.35, and layer thickness = 0.4 m (measured from the width of the fracture zone image on the televiewer log). The synthetic Stoneley waves from logs were also computed using these parameters. The overall match between the calculated deficit log (solid line) and the measured data (open circles) is quite good, especially for the upper part of the zone. Both logs show an average deficit of about 82% across the zone, which provides a measure of the overall fluid transmissivity across the fracture zone. The major difference between the two logs is at the lower part of the zone. The calculated amplitude shows a sharp decrease at the top (which is confirmed by the data). However, the amplitude decrease at the bottom part of the data is more gradual, while the calculated log from the homogeneous layer model predicts a sharp decrease. The sharp amplitude decrease at the top and the gradual decrease at the bottom, together with the fact that the reflection is seen clearly at the top but not at the bottom, led Paillet (1984) to hypothesize that the permeable fracture zone may have a non-uniform permeability distribution, and that the bottom part of the zone may be less permeable than the top part. With the heterogeneous permeable zone theory developed in this study, we can test this hypothesis by modeling the Stoneley wave transmission and reflection data using a variable permeability model for the fracture zone.

Although various permeability models can be chosen to model the Stoneley wave data, we use a simple permeability distribution model as shown in Figure 18. In this

model, the permeability is assumed to attain its maximum at the top boundary, and smoothly varies to zero at the bottom boundary $z = L = 0.4$ m. This variation is given as $k(z) = k_0[1 + cos(\frac{z}{L}\pi)]$ where k_0 is chosen by requiring that $\frac{1}{L}\int_0^L k(z)dz = 2.5$ Darcy, which gives $k_0 = 2.5$ Darcy. In this way, the total fluid transmissivity of the fracture zone remains the same as the homogeneous layer model. The top boundary has a sharp permeability contrast while the bottom boundary has no permeability contrast (Figure 18). In our numerical modeling, the other parameters used are the same as in the homogeneous layer model. In addition, because of the pressure of the logging tool, we use an effective borehole radius calculated using $\bar{R} = \sqrt{R^2 - R_{tool}^2}$.

For the permeability model in Figure 18, two numerical modeling experiments were performed. In the first experiment, the incident Stoneley wave approaches the heterogeneous zone from the bottom boundary ($z = L$) where there is no permeability contrast. This experiment is performed to simulate the logging operation of the acoustic logging tool that is being pulled towards the fracture zone from below the zone. For the second experiment, we let the incident Stoneley wave approach the model from the top boundary ($z = 0$), where there is a sharp permeability contrast. This experiment is performed to simulate the acoustic logging tool that has just passed through the fracture zone and is being pulled away from the zone. The downgoing Stoneley wave from the source will interact with the fracture zone and the resulting reflection will be recorded by the receiver.

Figure 19 shows the calculated transmission and reflection coefficients for the two numerical modeling experiments in the frequency range of $0 \sim 8$ kHz. The transmission coefficients for the two experiments are very close and are around the value of 0.43 at about 5 kHz. This will produce an amplitude deficit value of about $(1-0.43^2) \times 100\% \approx 0.82\%$, in excellent agreement with the measured value on the amplitude log. However, the reflection coefficients for the two experiments differ greatly at higher frequencies, although they approach each other towards the zero frequency (this suggests that the reflection data of very low frequency tube waves is not sensitive to the structure of the permeable zone, the same as shown in Figures 9, 11, and 13). For the Stoneley wave approaching the top boundary of the fracture zone (sharp permeability contrast boundary), the reflection coefficient is about 0.1, which is about the same order of magnitude as the observed reflected Stoneley wave amplitude shown in Figure 17. For the Stoneley wave approaching the bottom boundary (zero permeability contrast boundary), the reflection coefficient value around 5 kHz is only about 0.02. Given the noise level in the measured Stoneley waveform data in Figure 17, reflected waves with such a small amplitude cannot be visually identified. Thus, the variable permeability model shown in Figure 18 can model the reflection data very well.

To model the transmission data, we again need to use the finite difference method and the propagator matrix formulation result given in Equation (24). When the receiver of the logging tool enters the fracture zone (source below receiver), the Stoneley wave is attenuated because of the propagation loss due to permeability. This amplitude loss can be modeled by computing the Stoneley wave amplitude reduction from the bottom boundary to the receiver (assuming wave incidence from the bottom). In this way, amplitude loss as a function of the receiver location can be modeled. Similarly, when the source enters the permeable zone (receiver above the zone), the Stoneley

wave amplitude *vs.* source location can be simulated in a similar way (assuming wave incidence from the top boundary using reciprocity).

We again use the same variable permeability model shown in Figure 18. The simulated amplitude log (solid curve) for the permeability model in Figure 18 is plotted in Figure 20 with the measured amplitude log (dots) and the homogeneous layer model result (dashed curve). The homogeneous model results of Tang et al. (1991a) were measured from the synthetic seismograms shown in Figure 17 and were, therefore, able to model the small amplitude increase due to the superposition of the incident and reflected waves at the top fracture zone boundary.

Although our simulation result is modeled in the frequency domain for the central wave frequency of 5 kHz, the overall amplitude decrease across the fracture zone is not different from the time domain measurement of the waveforms. The major improvement by our heterogeneous permeability model is at the lower portion of the amplitude deficit log. Both the numerical result and the data show the same gradual change of amplitude when the receiver enters the fracture zone from the bottom boundary, while the homogeneous model result shows the same sharp amplitude change as at the top boundary. Therefore, by using the variable permeability model, we successfully explain that the gradual amplitude change at the lower boundary is due to the small permeability for the lower portion of the zone as compared to the upper portion. Thus, in addition to the agreement for the reflection data, the excellent agreement between theory and data for the transmission data again supports the interpretation of the fracture zone permeability distribution, as given by the variable permeability models (Figure 18).

The numerical modeling results confirm the hypothesis that the bottom part of the URL M11 well fracture zone is less permeable than the top part. This example also demonstrates how the numerical modeling approach can be used to assess the permeability heterogeneities of borehole permeability heterogeneity from logging data.

CONCLUSIONS

An effective numerical analysis method has been developed to handle Stoneley wave propagation through borehole heterogeneities. This technique is based on finite difference modeling of dynamic fluid flow in a heterogeneous formation and the propagation matrix method for wave propagation in a 1-D heterogeneous medium.

This technique can be used to calculate the effective Stoneley wave attenuation and velocity dispersion if the wave propagation distance is within the heterogeneous formation. When the heterogeneity variation is confined to a zone whose thickness is small compared to the propagation distance, the technique can be used to calculate the Stoneley wave transmission across the permeable zone and the reflection from the zone.

For continuous permeability variations, the cumulative Stoneley wave attenuation and velocity dispersion can be well described by a homogeneous permeability model having the average properties of the heterogeneous medium. For discontinuous variations, significant deviation from the homogeneous model results exists only when the

media has high permeability. The numerical modeling results demonstrate that, for most situations (low to medium permeability), the homogeneous model theory can be reliably used to obtain average permeability of a heterogeneous permeable formation.

For Stoneley wave transmission and reflection at a heterogeneous permeable structure, the transmitted wave amplitude is controlled by the overall fluid transmissivity of the structure, although some discrepancy may arise depending on the structure of the heterogeneities. Reflection, on the other hand, is most sensitive to the structure of the heterogeneities. However, at very low frequencies, both transmission and reflection are controlled by the overall fluid transmissivity of the structure, irrespective of the distribution of heterogeneities within the structure. This shows that the low frequency tube wave can be used as an effective means to measure fluid transmissivity of the permeable structure. The Stoneley wave reflection at higher frequencies can be used to detect heterogeneity variation within the structure.

The numerical modeling results have been verified by both laboratory experimental data and field acoustic logging data. Thus, for problems concerning acoustic logging in heterogeneous porous formations, the numerical method can be effectively used to help determine formation permeability heterogeneities and their fluid transmissivity.

ACKNOWLEDGEMENTS

This research was supported by the Borehole Acoustics and Logging Consortium at M.I.T. and by Department of Energy Grant DE-FG02-86ER13636.

Table I. Physical properties of sample B in Winkler et al.'s (1989) experiments

$\phi(\%)$	κ_0(mD)	τ	ρ_0(kg/m^3)	μ(cp)	V_f(m/s)	ρ_e(kg/m^3)	V_p(m/s)	V_s(m/s)
22.9	2300	2.4	934	9.34	999	1960	2930	1610

APPENDIX

Finite Difference Solution of Dynamic Fluid Flow in (r, z) Coordinates

In borehole acoustic logging in formations whose heterogeneity variation is in the radial (r) and vertical (z) directions, the (r, z) coordinates finite difference scheme is used to solve for the fluid flow in the heterogeneous medium. For the cylindrical system, the governing equation is given by Equation (9):

$$\frac{\partial}{\partial r}\left(\alpha(r,z)\frac{\partial p}{\partial r}\right)+\frac{\alpha(r,z)}{r}\frac{\partial p}{\partial r}+\frac{\partial}{\partial z}\left(\alpha(r,z)\frac{\partial p}{\partial z}\right) \quad + \quad i\omega p = 0 \qquad (A.1)$$

$$(R_0 < r < R \text{ and } 0 < z < L)$$

where R_0 is the borehole radius, R is a large radial distance $(R >> R_0)$ at which p is effectively zero, and $z = 0$ and $z = L$ represent the lower and upper boundaries of the heterogeneous formation, respectively. Equation(A.1) can be non-dimensionalized to become (see Zhao et al., 1993)

$$\frac{\partial}{\partial r'}\left(\alpha'\frac{\partial p}{\partial r'}\right)+\frac{R-R_0}{R_0+(R-R_0)r'}\alpha'\frac{\partial p}{\partial r'}+\frac{(R-R_0)^2}{L^2}\frac{\partial}{\partial z'}\left(\alpha'\frac{\partial p}{\partial z'}\right)+i\beta p=0 \qquad (A.2)$$

where

$$\alpha' = \frac{\gamma(r,z)}{\left[1-\frac{i}{2}\tau\kappa_{max}\gamma(r,z)\frac{\rho_f\omega}{\mu}\phi\right]^{1/2}-i\tau\kappa_{max}\gamma(r,z)\frac{\rho_f\omega}{\mu\phi}} \quad , \qquad (A.3)$$

is the non-dimensionalized dynamic fluid diffusivity, $\gamma(r,z)=\frac{\kappa(r,z)}{\kappa_{max}}$ is the dimensionless permeability distribution in the (r, z) coordinated, κ_{max} being the maximum permeability in the model, and $\beta = \omega(R-R_0)^2/\alpha_0$, where $\alpha_0 = \frac{\kappa_{max}K_f}{\mu\phi}$ is the maximum fluid diffusivity in the model. The dimensionless spatial variables are given by

$$\begin{aligned} r' &= \frac{r-R_0}{R-R_0} \quad (0<r'<1) \\ z' &= z/L \quad (0<z'<1) \quad . \end{aligned}$$

Solution of Equation (A.2) can be obtained as the steady-state solution of the following equation,

$$\Gamma p = \frac{\partial p}{\partial t'} \qquad (A.4)$$

where Γp is the left hand side of Equation (A.2), and t' is a dimensionless time. The steady-state solution is found by employing a stable iterative procedure using the ADI method. The variables r', z', and t' are discretized as

$$\begin{cases} r' = i\Delta r' & i = 0,1,2,\cdots,I \quad \Delta r' = 1/I \\ z' = j\Delta z' & j = 0,1,2,\cdots,J \quad \Delta z' = 1/J \\ t' = n\Delta t' & n = 0,1,2,\cdots,N \end{cases} \qquad (A.5)$$

where $\Delta t'$ can be chosen as $\sqrt{(\Delta r'^2 + \Delta z'^2)}/2$.

To use the ADI method to solve Equation (A.4), we re-write this equation in the form of

$$p_{t'} = \Lambda_1 p + \Lambda_2 p \ . \tag{A.6}$$

where,

$$\begin{cases} \Lambda_1 p = \dfrac{\partial}{\partial r'}\left(\alpha' \dfrac{\partial p}{\partial r'}\right) + \dfrac{R - R_0}{R_0 + (R - R_0) r'} \alpha' \dfrac{\partial p}{\partial r'} + i\beta p \\ \Lambda_2 p = \dfrac{(R - R_0)^2}{L^2} \dfrac{\partial p}{\partial z'}\left(\alpha' \dfrac{\partial p}{\partial z'}\right). \end{cases} \tag{A.7}$$

The ADI finite difference form of Equation (A.6) is

$$\left(I - \frac{\Delta t'}{2}\Lambda_{1h}\right) p^{n+1/2} = \left(I + \frac{\Delta t'}{2}\Lambda_{2h}\right) p^n \tag{A.8}$$

$$\left(I - \frac{\Delta t'}{2}\Lambda_{2h}\right) p^{n+1} = \left(I + \frac{\Delta t'}{2}\Lambda_{1h}\right) p^{n+1/2} \tag{A.9}$$

where Λ_{1h} and Λ_{2h} are finite difference operators:

$$\begin{aligned} \Lambda_{1h} p &= \frac{1}{\Delta r'^2}\Big[(B_{i,j} - D_{i,j}) p_{i-1,j} - (B_{i,j} + B_{i+1,j} - D^{(1)}_{i,j} \\ &\quad - i\beta\Delta r'^2) p_{i,j} + B_{i+1,j} p_{i+1,j}\Big] \end{aligned} \tag{A.10}$$

$$\Lambda_{2h} p = D^{(2)}_{i,j} \frac{1}{\Delta z'^2}\left[C_{i,j} p_{i,j-1} - (C_{i,j} + C_{i,j-1}) p_{i,j} + C_{i,j+1} p_{i,j+1}\right] \ , \tag{A.11}$$

where

$$\begin{cases} A_{i,j} = \alpha'_{i,j} \\ B_{i,j} = \dfrac{A_{i,j} + A_{i-1,j}}{2} \\ C_{i,j} = \dfrac{A_{i,j} + A_{i,j-1}}{2} \\ D^{(1)}_{i,j} = \dfrac{(R - R_0) B_{i,j} \Delta r'}{[R_0 + (R - R_0)(r'_{i,j} + r'_{i-1,j})/2]} \\ D^{(2)}_{i,j} = \dfrac{(R - R_0)^2}{L_2}. \end{cases} \tag{A.12}$$

Therefore, the finite difference form of Equations (A.10) and (A.11) is

$$\begin{aligned} &-\mu_1 (B_{i,j} - D^{(1)}_{i,j}) p^{n+1/2}_{i-1,j} + \Big[1 + \mu_1\Big(B_{i,j} + B_{i+1,j} - D^{(1)}_{i,j} \\ &\qquad - i\beta\Delta r'^2)\Big] p^{n+1/2}_{i,j} - \mu_1 B_{i+1,j} p^{n+1/2}_{i+1,j} \\ &= \mu_2 D^{(2)}_{i,j} p^n_{i,j-1} + \Big[1 - (C_{i,j} + C_{i,j+1}) \mu_2 D^{(2)}_{i,j}\Big] p^n_{i,j} + \mu_2 D^{(2)}_{i,j} C_{i,j+1} p^n_{i,j+1} \end{aligned} \tag{A.13}$$

$$\begin{aligned} &-\mu_2 D^{(2)}_{i,j} C_{i,j} p^{n+1}_{i,j-1} + \Big[1 + \mu_2 D^{(2)}_{i,j}(C_{i,j} + C_{i,j+1})\Big] p^{n+1}_{i,j} - \mu_2 D^{(2)}_{i,j} C_{i,j+1} p^{n+1}_{i,j+1} \\ &= \mu_1 (B_{i,j} - D^{(1)}_{i,j}) p^{n+1/2}_{i-1,j} + \Big[1 - \mu_1\Big(B_{i,j} + B_{i+1,j} - D^{(1)}_{i,j} \\ &\quad - i\beta\Delta r'^2)\Big] p^{n+1/2}_{i,j} + \mu_1 B_{i+1,j} p^{n+1/2}_{i+1,j} \end{aligned} \tag{A.14}$$

where

$$\mu_1 = \frac{\Delta t'}{2\Delta r'^2} \qquad \text{and} \qquad \mu_2 = \frac{\Delta t'}{2\Delta z'^2}.$$

The boundary conditions for the problem are given in Equations (11), (12), and (13), which in the finite difference form, are given by

$$\begin{cases} p(0,j) = p_0 exp\{ik_e \Delta z' j\} \\ p(R,j) = 0 \ . \end{cases} \qquad (0 < j < J) \qquad \text{(A.15)}$$

and

$$\begin{cases} p(i,0) = p(i,1) \\ p(i,J-1) = p(i,J) \end{cases} \qquad (0 < i < I) \ . \qquad \text{(A.16)}$$

The finite difference Equations (A.13) and (A.14), together with the boundary conditions, can be solved using Thomas algorithm (see Zhao *et al.*, 1993 and Ferziger, 1980).

REFERENCES

Aki, K., and P.G. Richards, 1990, *Quantitative Seismology*, W.H. Freeman and Co., New York.

Cheng, C.H., and M.N. Toksöz, 1981, Elastic wave propagation in a fluid-filled borehole and synthetic acoustic logs, *Geophysics, 46*, 1042–1053.

Ferziger, J.H., 1981, *Numerical Methods for Engineering Applications*, John Wiley & Sons, Inc., New York.

Güler, F., and M.N. Toksöz, 1987, Ultrasonic laboratory study of full waveform acoustic logs in boreholes with fractures, *M.I.T. Full Waveform Acoustic Logging Consortium Annual Report.*

Hornby, B.E., D.L. Johnson, K.H. Winkler, and R.A. Plumb, 1989, Fracture evaluation using reflected Stoneley-wave arrivals, *Geophysics, 54*, 1274–1288.

Johnson, D.L., J. Koplik, and R. Dashen, 1987, Theory of dynamic permeability and tortuosity in fluid-saturated porous media. *J. Fluid Mech., 176*, 379–400.

Kostek, S., 1991, Borehole acoustic wave propagation in the presence of fractures: A finite difference approach, *SEG 61st Ann. Intl. Mtg. & Expo. Expanded Abst.* Houston, Texas.

Kostek, S., 1990, Modeling of elastic wave propagation in a fluid-filled borehole excited by a piezoelectric transducer, *Master's thesis*, M.I.T., Cambridge.

Norris, A.N., 1989, Stoneley-wave attenuation and dispersion in permeable formations, *Geophysics, 54*, 330–341.

Paillet, F.L., 1980, Acoustic propagation in the vicinity of fractures which intersect a fluid-filled borehole, *Trans., Soc. Prof. Well Log Analysts, 21st Ann. Symp.*, paper DD.

Paillet, F.L., 1984, Field test of a low-frequency sparker source for acoustic waveform logging, *M.I.T. Full Waveform Acoustic Logging Consortium Annual Report*, 207–228.

Tang, X.M., and C.H. Cheng, 1988, Wave propagation in a fluid-filled fracture: An experimental study, *Geophys. Res. Ltt., 15*, 1463–1466.

Tang, X.M., C.H. Cheng, and F.L. Paillet, 1991a, Modeling Stoneley wave Propagation across in-situ fractures, *Trans. 36th Soc. Prof. Well Log Analysis*, Paper GG.

Tang, X.M., C.H. Cheng, and M.N. Toksöz, 1991b, Danymic permeability and dorehole Stoneley waves: A simplified Biot-Rosenbaum model, *J. Acous. Soc. Am., 90*, 1632–1646.

Tang, X.M., and C.H. Cheng, 1993, Borehole Stoneley wave propagation across heterogeneous and permeable structures, *Geophysical Prospecting, 41*, 165–187.

Winkler, K.W., H.L. Liu, and D.L. Johnson, 1989, Permeability and borehole Stoneley waves: Comparison between experiment and theory, *Geophysics, 54*, 66–75.

Zhao, X.M., and M.N. Toksöz, 1991, Modeling fluid flow in heterogeneous and anisotropic porous media, *M.I.T. Full Waveform Acoustic Logging Consortium*, 245–270.

Zhao, X.M., C.H. Cheng., X.M. Tang, and M.N. Toksöz, 1992, Dynamic fluid flow in heterogeneous porous media and through a single fracture with rough surfaces, *M.I.T. Borehole Acoustics and Logging Consortium*, 157–178.

Zhao, X.M., M.N. Toksöz, and C.H. Cheng, 1993, Stoneley wave propagation in heterogeneous porous formations, *M.I.T. Borehole Acoustic and Logging Consortium*, 43–78.

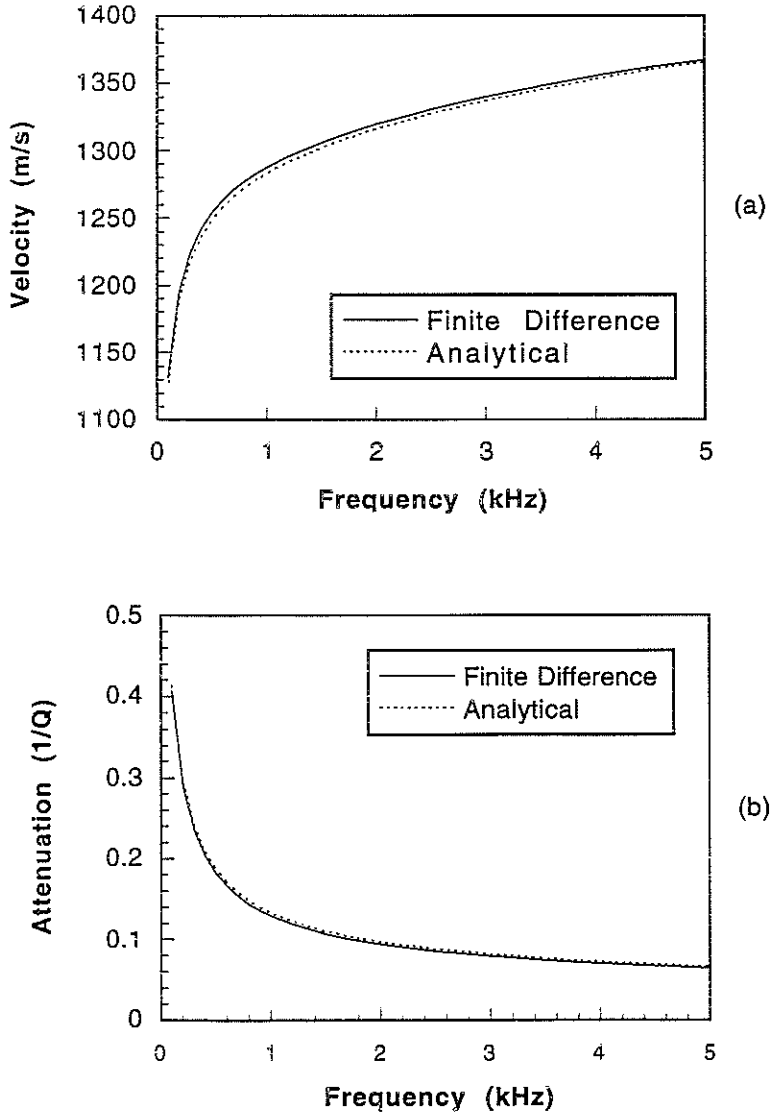

Figure 1: Comparison between analytical (dashed curves) and finite difference (solid curves) results: (a) Stoneley wave velocity, (b) Stoneley wave attenuation.

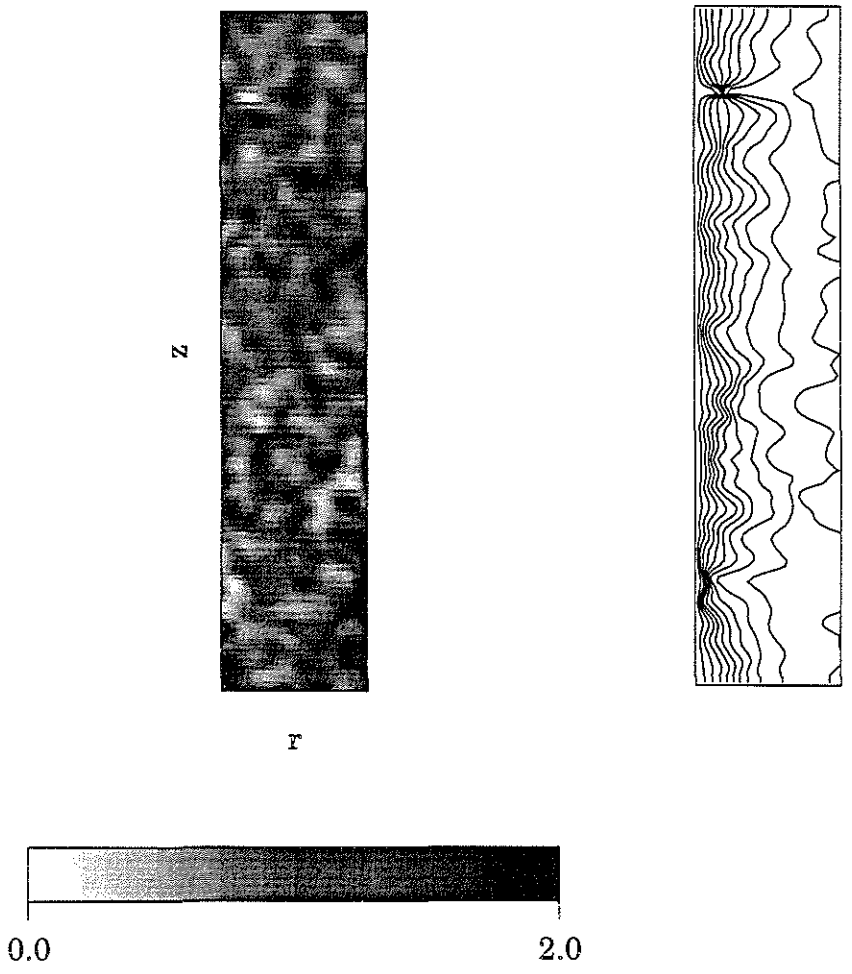

Figure 2: Random permeability model (left) generated using 2-D Gaussian correlation function and simulated pore fluid pressure contour (right) in the formation for a 100 Hz Stoneley wave. The model dimensions are: 10 m in the z-direction and 1 m in the r-direction. Permeability ranges from 0 - 2 Darcy.

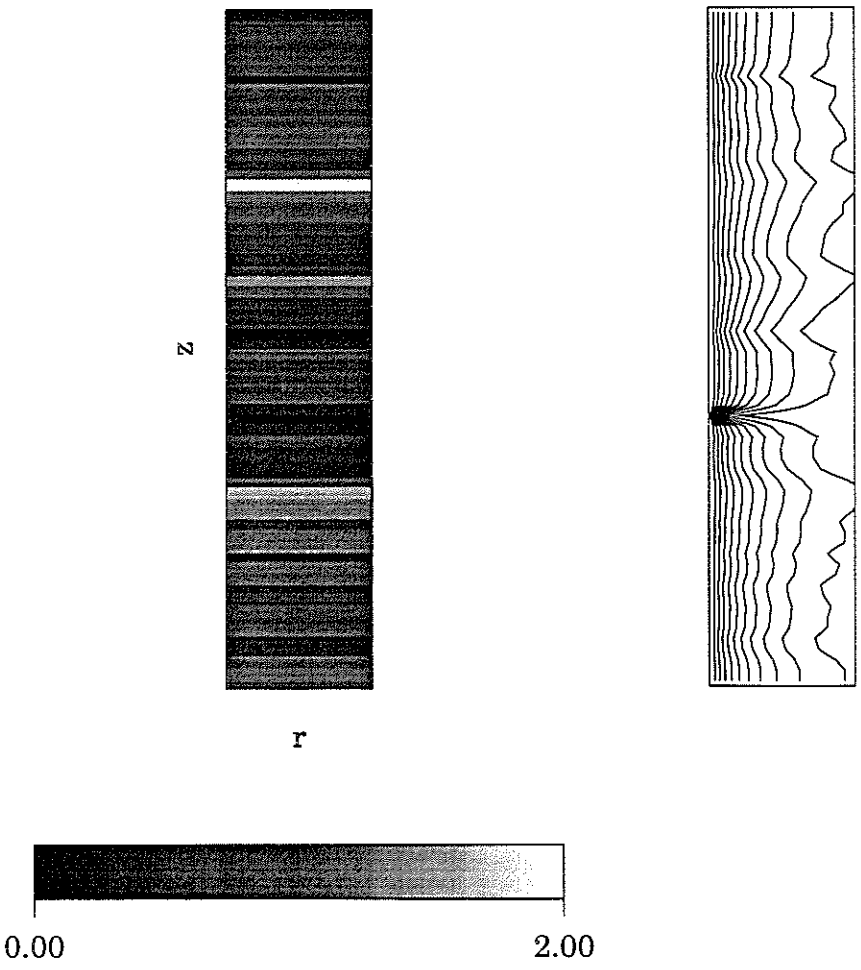

Figure 3: 1-D permeability model (left) with a Gaussian correlation function and simulated pore fluid pressure contour (right) for a 100 Hz Stoneley wave. Model dimensions are the same as in Figure 2.

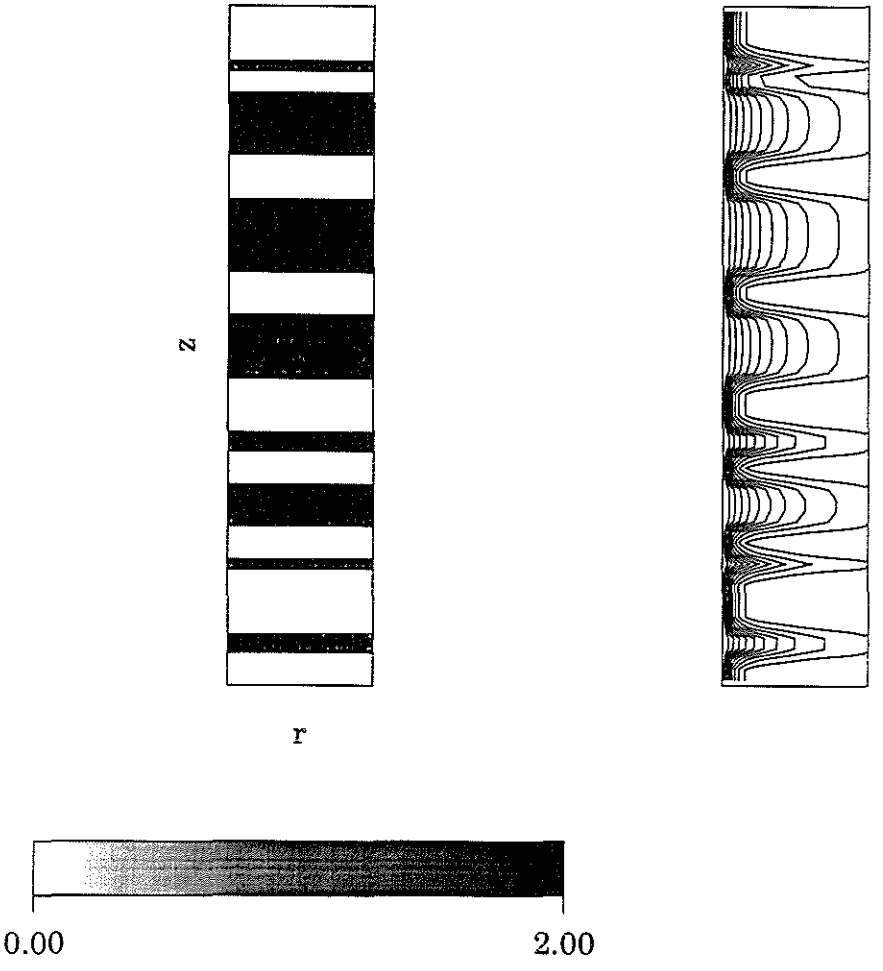

Figure 4: Cyclic permeability model (left) and the simulated pore pressure contour (right) for a 100 Hz Stoneley wave. Model dimensions are the same as in Figure 2.

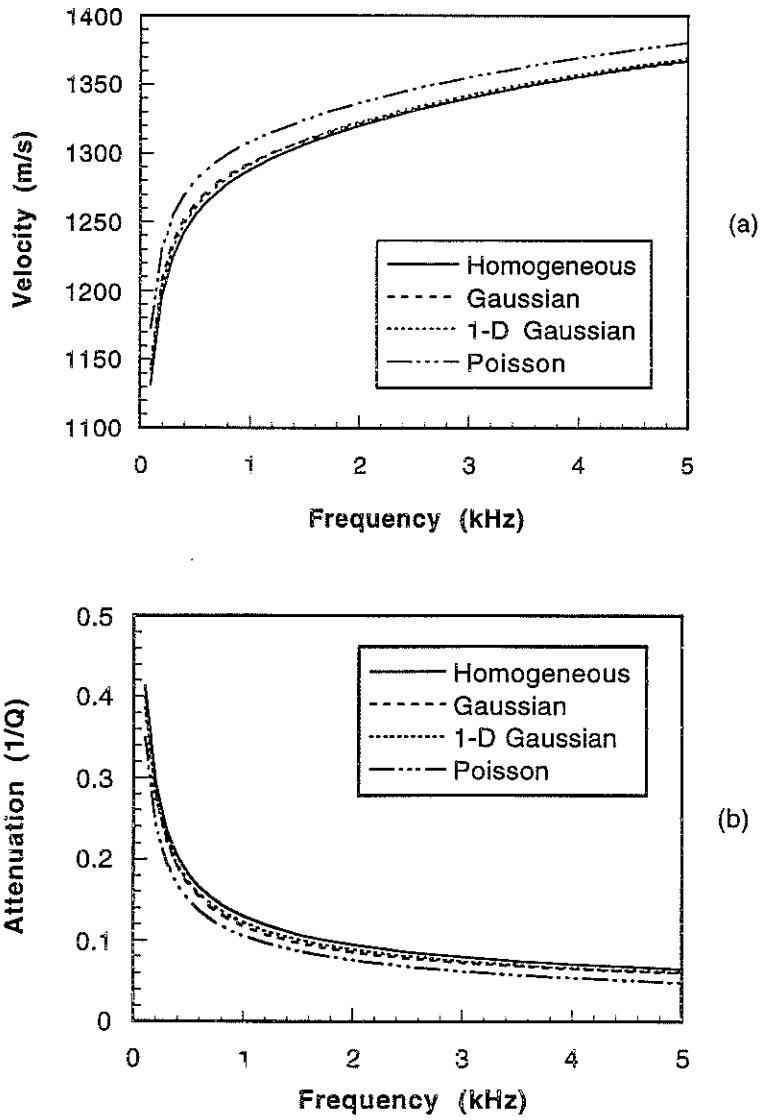

Figure 5: Stoneley wave phase velocity (a) and attenuation (b) curves for different heterogeneous permeability models. The average permeability of the models is 1 Darcy.

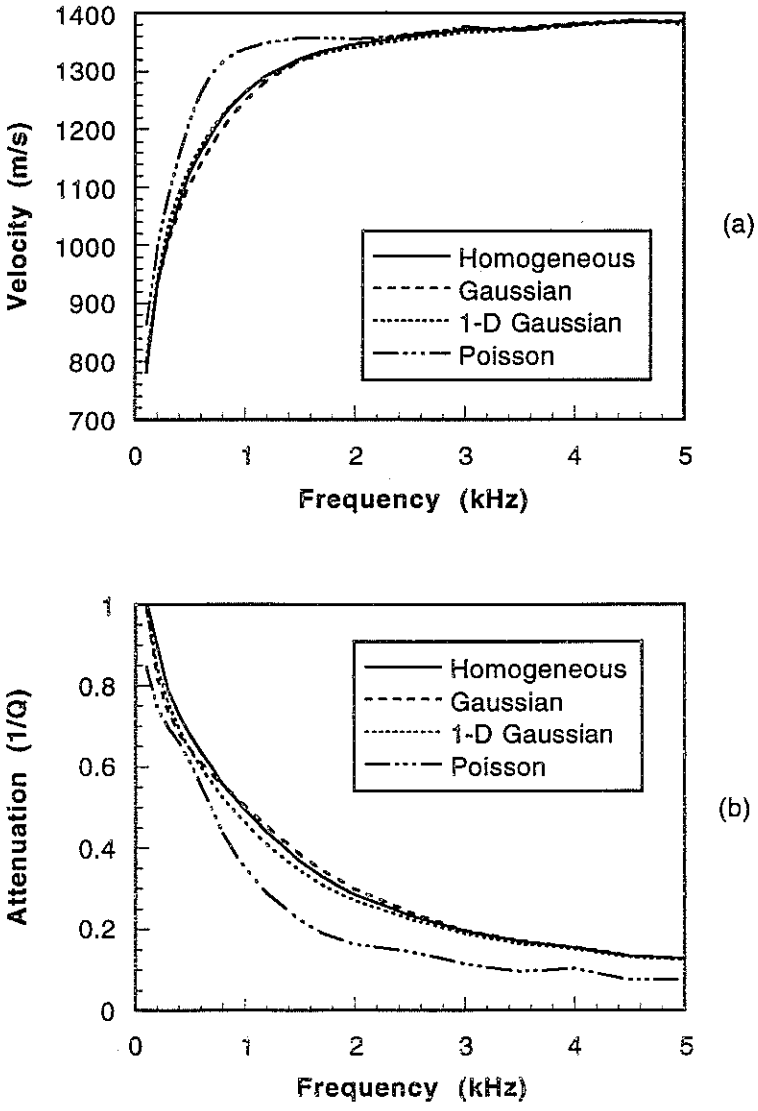

Figure 6: Stoneley wave phase velocity (a) and attenuation (b) curves for different heterogeneous permeability models. The average permeability of the models is 10 Darcy.

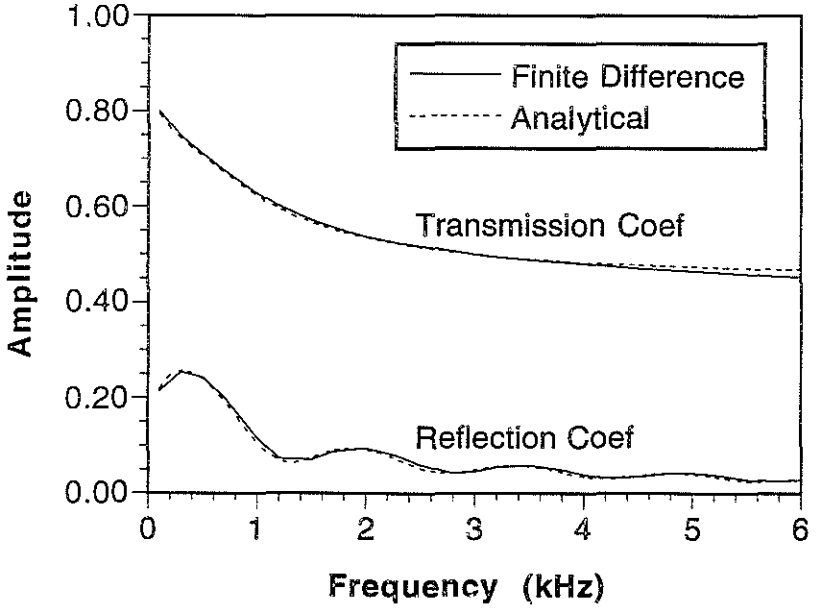

Figure 7: Testing the results of numerical modeling of Stoneley wave propagation across a permeable zone (solid curves) using the analytical solution results (dashed curves).

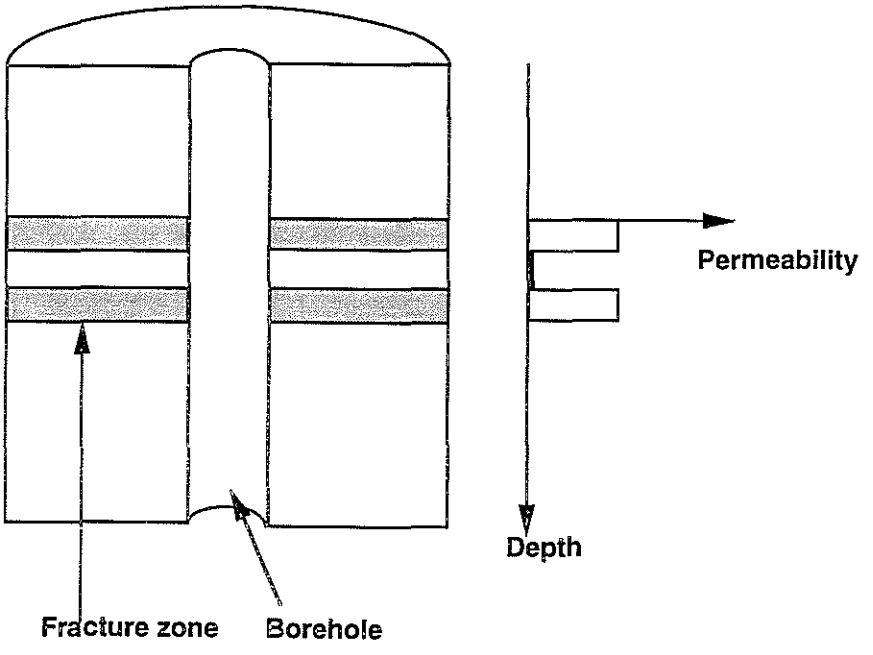

Figure 8: Double permeability layer model for modeling Stoneley wave propagation. Two layers of 10 Darcy permeability and 0.15 m thickness are separated by a non-permeable formation of 0.2 m thick.

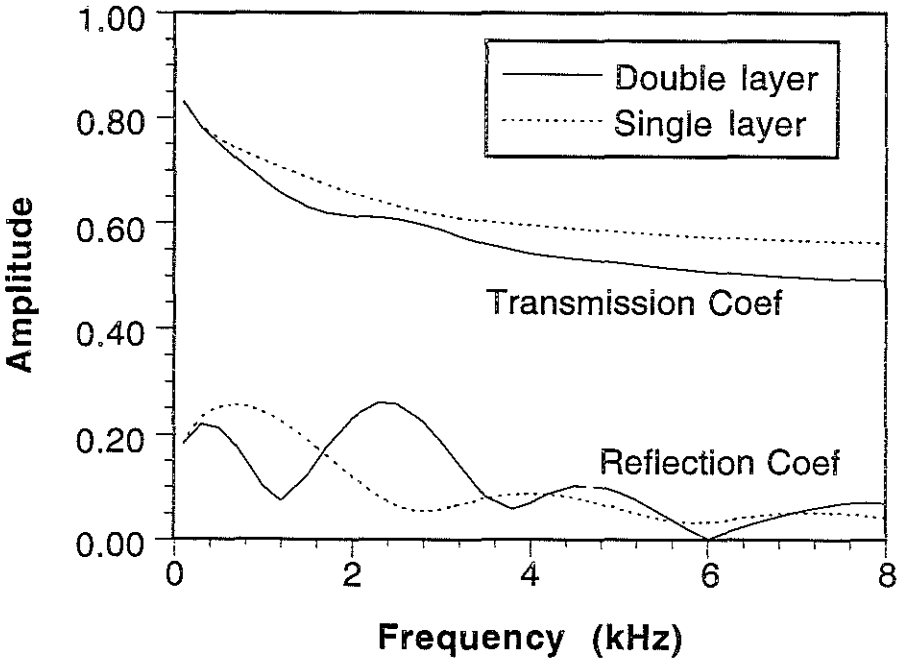

Figure 9: Stoneley wave transmission and reflection coefficients (solid curves) for the double layer model shown in Figure 8. For comparison, the results for a homogeneous layer with cumulative thickness of 0.3 m and 10 Darcy permeability are also shown (dashed curves). The two results agree only in the low frequency limit.

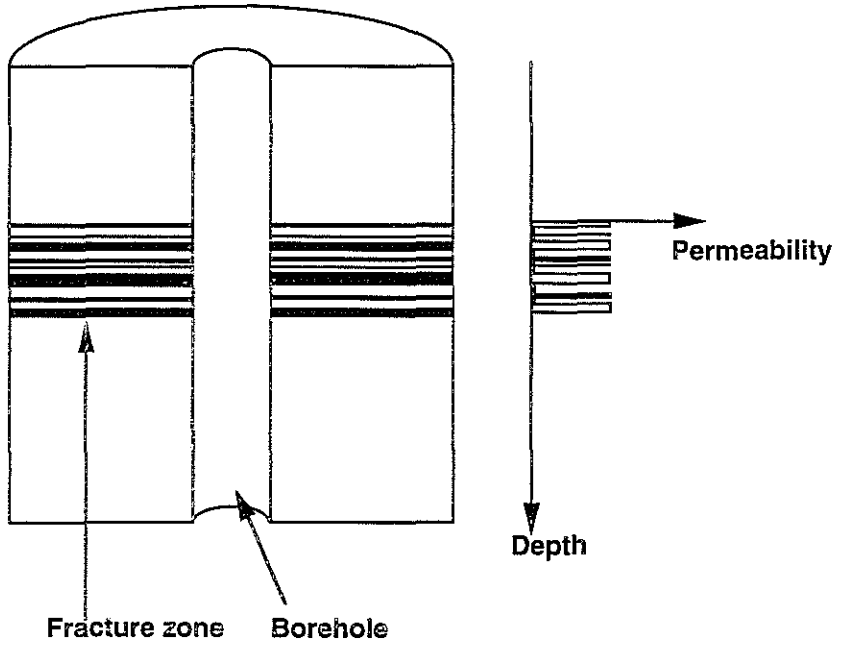

Figure 10: Multiple layer permeable zone model. The thickness and average permeability of the zone are 0.4 m and 10 Darcy, respectively.

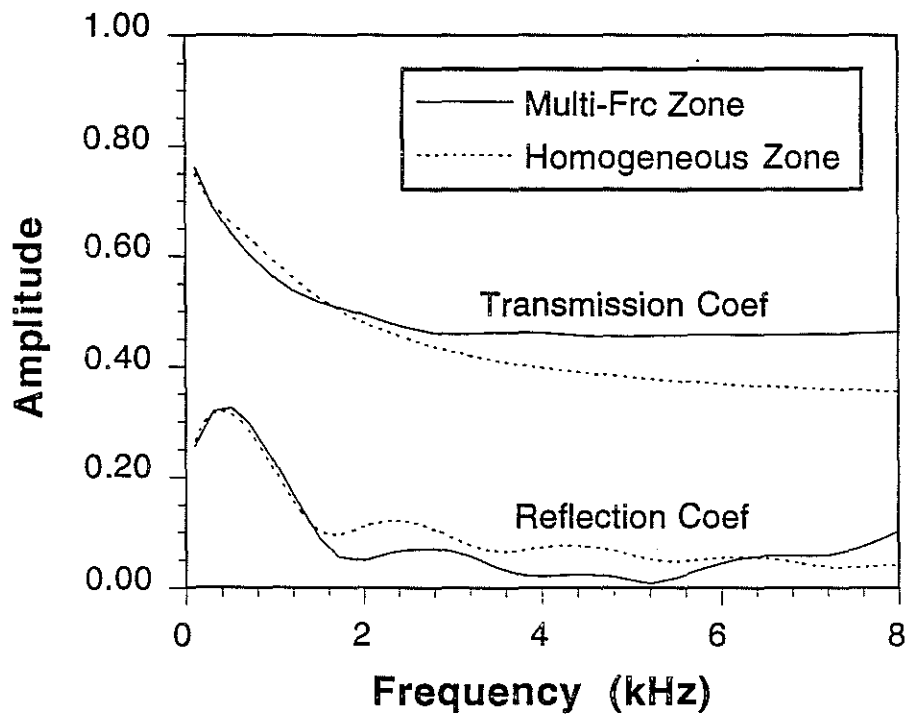

Figure 11: Stoneley wave transmission and reflection coefficients for the multiple layer zone model (solid curves) shown in Figure 10. For comparison, the results for a homogeneous zone of thickness 0.4 m and permeability 10 Darcy are also shown (dashed curves).

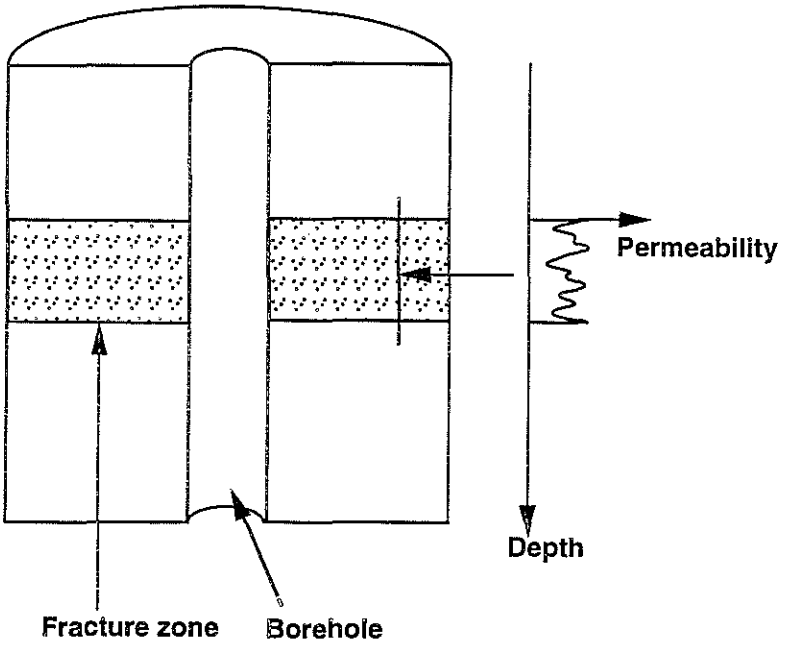

Figure 12: Permeability zone model with random permeability variation along the borehole axial direction. The variation is characterized by Gaussian correlation function. The average permeability of the model is 10 Darcy.

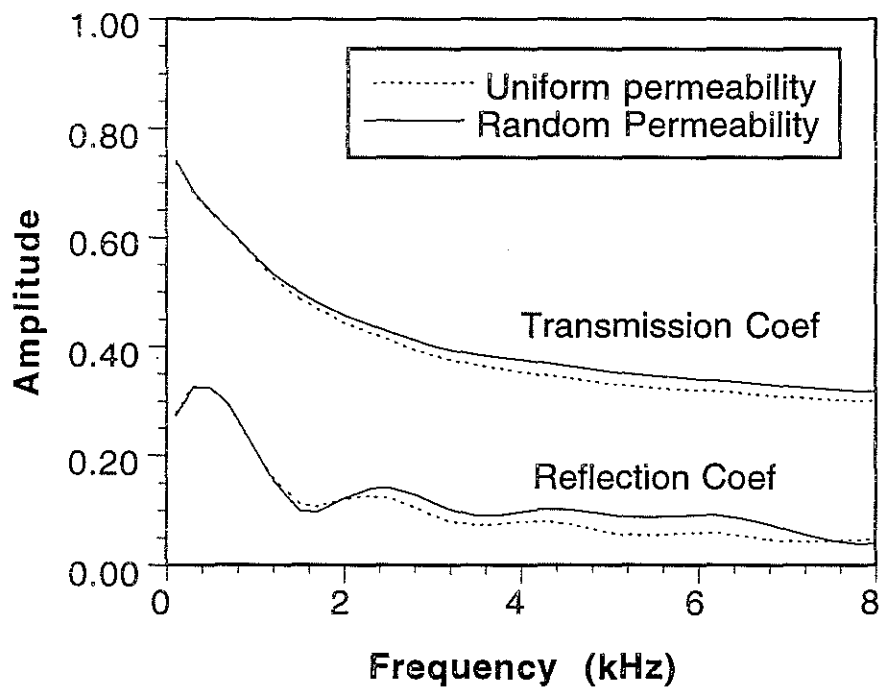

Figure 13: Stoneley wave transmission and reflection coefficients (solid curves) for the random permeability model of Figure 12. The results for a uniform permeability (10 Darcy) layer are also shown (dashed curves).

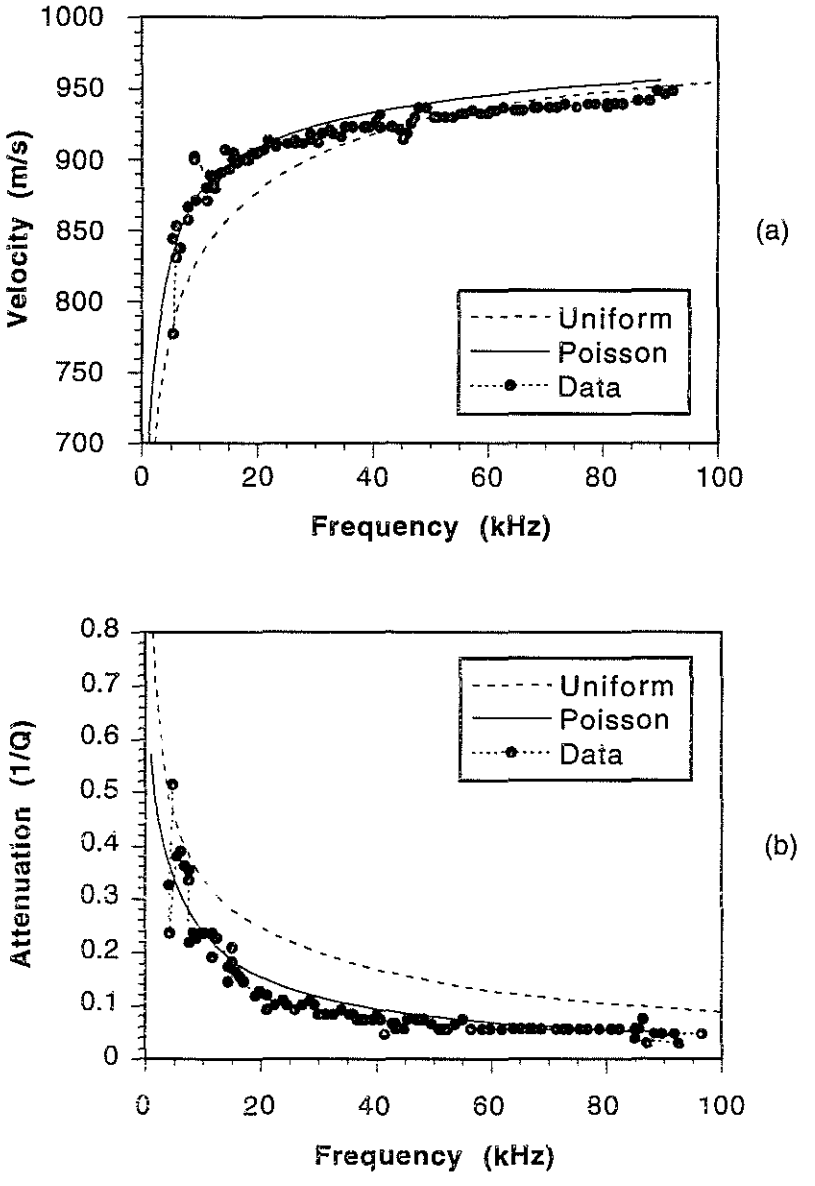

Figure 16: Comparison of the experimental Stoneley wave velocity (a) and attenuation (b) data (dots) with the theoretical modeling results (solid curves) using the discontinuous permeability layer model. There is an excellent agreement between data and theory for both velocity and attenuation.

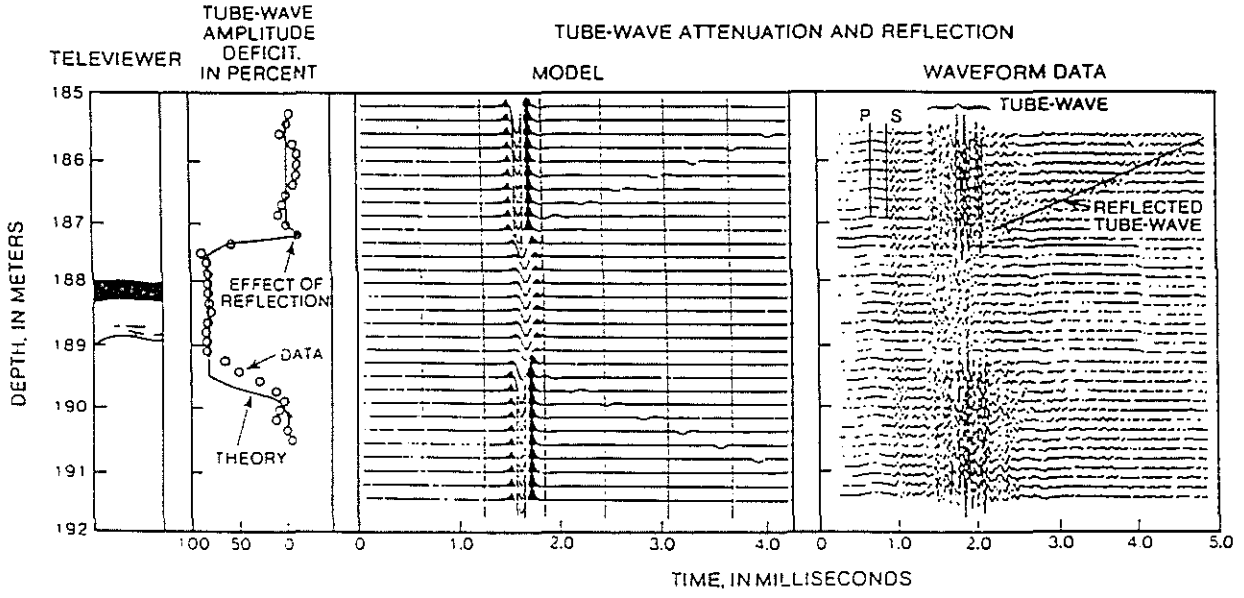

Figure 17: Stoneley waveforms, amplitude log, and televiewer log for the URL-M11 well around 188 m (After Paillet, 1984). The theoretical modeling results of Tang et al. (1991a) are also shown in this figure.

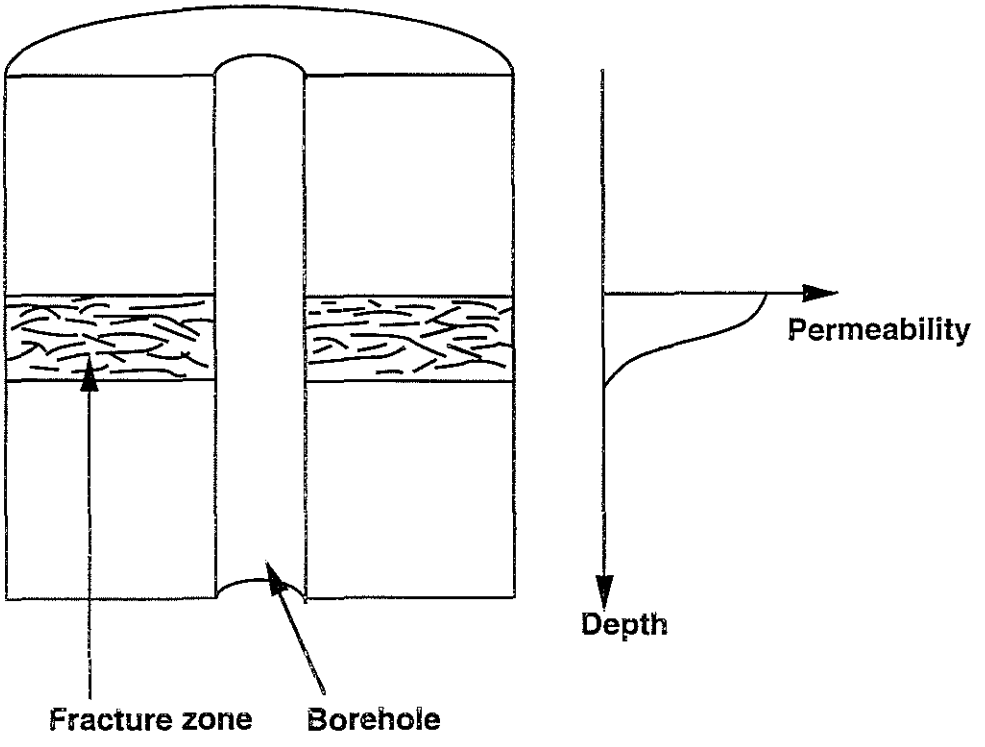

Figure 18: Variable permeability model for the URL-M11 fracture zone. The permeability is the highest (2.5 Darcy) at the top boundary, and decreases to attain a zero value at the lower boundary.

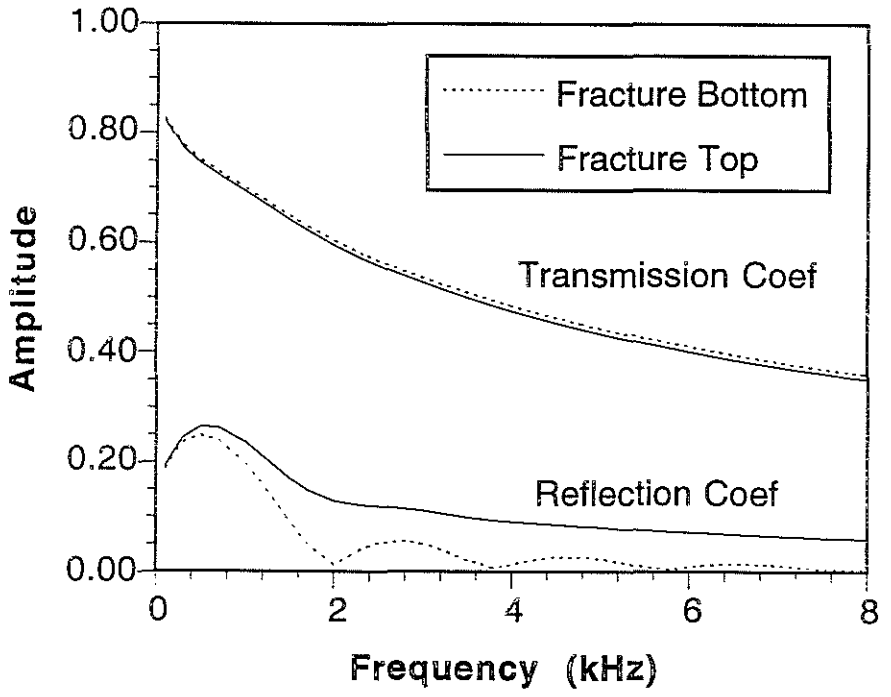

Figure 19: Simulated Stoneley wave (5 kHz) transmission and reflection coefficients using the model shown in Figure 18. The dashed (solid) curves correspond to the situation in which the logging tool is below (above) the fracture zone and the wave is incident from the bottom (top) of the fracture zone. The transmission coefficients for the two cases are very close, while the reflection coefficients from the fracture top boundary are much greater than those from the bottom boundary. This agrees with the non-symmetric reflection patterns of the fracture zone (Figure 17).

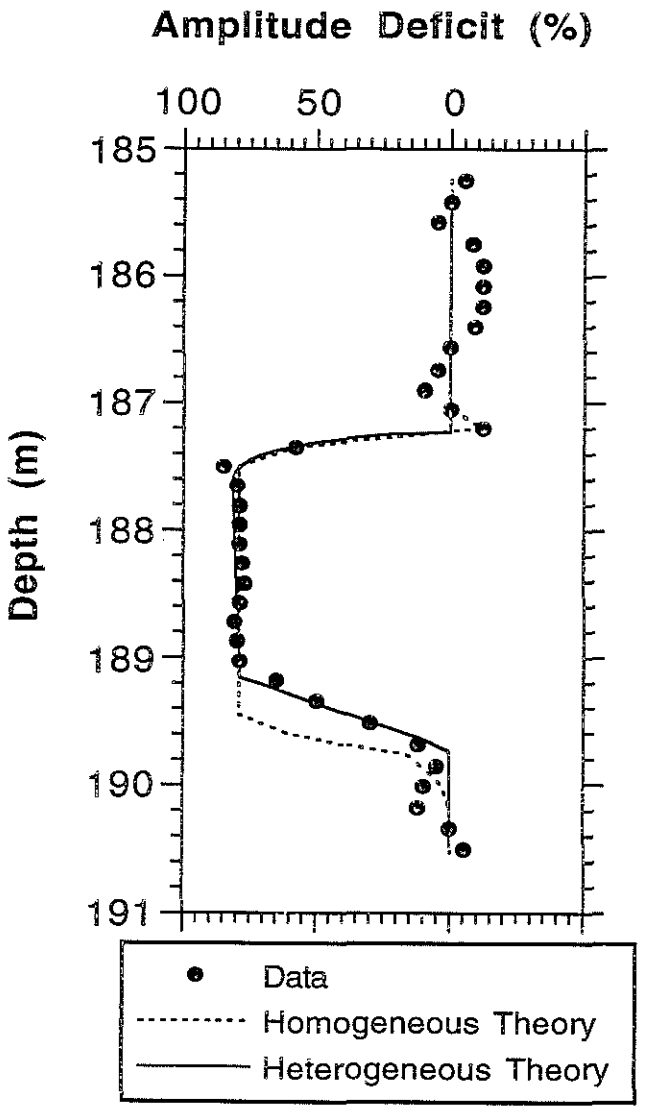

Figure 20: Amplitude deficit log from the measured Stoneley wave data (dots), the homogeneous layer modeling (dashed curve), and the heterogeneous permeability zone modeling. For the same fluid transmissivity, both theories match the portion of the data where the attenuation is the greatest (fracture zone between source and receiver). However, for the lower portion of the amplitude deficit log where the receiver is within the fracture zone, only the heterogeneous model results agree with the data.